# Literature Review on Heat Transfer Fluids and Thermal Energy Storage Systems in CSP Plants

**STERG Report**

Lukas Heller*

May 31, 2013

## Contents

**1. Introduction** **4**
1.1. Scope . . . . . 4

**I. Heat Transfer Fluids** **5**

**2. Qualities of HTFs** **5**

**3. Liquids** **5**
3.1. Synthetic Oil . . . . . 5
3.2. Molten Salts . . . . . 6
3.3. Liquid Metals . . . . . 8
3.3.1. Sodium . . . . . 9
3.3.2. NaK . . . . . 10
3.3.3. LBE . . . . . 11
3.3.4. Summary Liquid Metals . . . . . 11
3.4. Liquid Glasses . . . . . 11

**4. Gases** **11**
4.1. Air . . . . . 12
4.2. Other Gases . . . . . 14
4.3. Summary Gaseous HTFs . . . . . 14

*Lukas_Heller@gmx.de - Solar Thermal Energy Research Group, Stellenbosch University

**5. Solids** **14**
5.1. Particle Receiver . . . . . 14

**6. Fluids with Phase Change** **15**
6.1. Direct Steam Generation (DSG) . . . . . 15

**7. Supercritical Fluids** **16**
7.1. s-$H_2O$ . . . . . 16
7.2. s-$CO_2$ . . . . . 17

**II. Thermal Energy Storage Systems** **22**

**8. Introduction** **22**

**9. Media for Active Sensible Heat TESSs** **24**
9.1. Storage Media in Use . . . . . 24
9.2. Molten Salts . . . . . 25
9.3. Sodium . . . . . 25
9.4. Haloglass™ RX . . . . . 26
9.5. Steam/Water . . . . . 26

**10. Media for Passive Sensible TESS/Filler Material** **27**
10.1. Packed Beds . . . . . 27
10.2. Rocks and Sand . . . . . 28
10.3. Concrete . . . . . 30
10.4. Ceramics . . . . . 31
10.5. Graphite . . . . . 31

**11. Latent Heat Storage Media** **32**
11.1. Salts . . . . . 33
11.2. Metals . . . . . 34

**12. Chemical Potential Storage Media** **35**

**13. System Considerations** **36**

**14. Modeling of TESS** **37**

**References** **40**

**Appendices** **55**

**A. Properties of HTFs** **56**
A.1. Overview . . . . . 56
A.2. Synthetic Oil Therminol® VP-1/Dowtherm® A . . . . . 59

A.3. Solar Salt™ . . . 60
A.4. HITEC® Heat Transfer Salt . . . 61
A.5. Low Temperature Salt . . . 62
A.6. High Temperature Salts . . . 63
A.7. Sodium . . . 65
A.8. Eutectic Sodium-Potassium Alloy . . . 66
A.9. Eutectic Lead-Bismuth Alloy . . . 67
A.10. Ambient Air . . . 68
A.11. Pressurized Air . . . 69
A.12. DSG - Superheated . . . 70
A.13. Supercritical $H_2O$ . . . 71
A.14. Supercritical $CO_2$ . . . 72

**B. Storage Media** **73**
B.1. Potential Sensible Heat Storage Media . . . 73
B.1.1. Haloglass™ RX . . . 77
B.2. PCMs with $T_{\mathrm{melt}} > 550\,^{\circ}\mathrm{C}$ . . . 78

## Nomenclature

CR(S) central receiver (system)

CSP concentrating solar power

DNI direct normal irradiation

DSG direct steam generation

HTF heat transfer fluid

LCOE levelized cost of electricity

LHTESS latent heat thermal energy storage system

PCM phase change material

TES(S) thermal energy storage (system)

# 1. Introduction

Concentrating Solar Power (CSP) plants generate electricity by concentrating direct normal irradiation (DNI) from the sun through mirror systems on receivers and converting the gained thermal energy into electricity in a heat engine. The main advantage of CSP as compared to other renewable energy technologies (like, for example, wind power and photovoltaics) is the possibility of relatively cheap and efficient storability and therefore dispatchability of energy. This is due to the conversion of the incoming radiation into thermal energy, which can be stored cost-efficiently.

On the other hand, this conversion means that CSP plants have thermodynamic cycles that limit their efficiency by the high and low temperature of the Carnot cycle. In order to achieve high conversion efficiencies, high temperatures at the heat engine energy source and low temperatures at its energy sink are necessary. These temperatures are limited by the heat transfer fluid (HTF) in the receiver and the working fluid in the heat engine cycle (which can be one and the same). Storage options have to be chosen according to the desired temperature range(s) of the HTF and the properties of the working fluid.

## 1.1. Scope

The scope of this review is to give an overview on research which has been done on HTFs for CSP plants and on media being utilized in thermal energy storage systems (TESS). The focus hereby is on high-efficiency/high-temperature cycles with large thermal energy storage systems—and therefore central receiver systems (CRS).

# Part I.
# Heat Transfer Fluids

## 2. Qualities of HTFs

HTFs can be classified by their states of matter during normal operating conditions. Additionally to the three standard states (gaseous, liquid, solid), HTFs that undergo a phase change and supercritical fluids are also possible.

Becker (1980) rated potential HTFs for CSP applications by their thermal and transport properties. After a first assessment, he focused on a commercial molten salt (*HITEC® Heat Transfer Salt*), a commercial heat transfer oil, air, hydrogen, helium, water vapor, sodium, potassium, mercury and ammonia. Cabeza et al. (2012) summarized the state of the art and the conducted research mostly on TESS for CSP applications. However, Cabeza et al. also looked at the heat transfer to and from the storage system and, therefore, the available heat transfer fluids.

Important thermophysical properties of HTFs are:

- low lower temperature limitation (solidification temperature)
- high upper temperature limitation (evaporation temperature/thermal stability limit) at low pressures
- high thermal conductivity → receiver temperature close to HTF temperature
- low viscosity → lower pumping power requirements
- high density and heat capacity → enable use as storage medium
- possibility of usage as working fluid
- chemical compatibility (low corrosivity) with contact materials
- low cost, high availability
- low toxicity, flammability, explosivity and environmental hazard

## 3. Liquids

### 3.1. Synthetic Oil

Almost all commercial parabolic trough CSP plants to date use oil as the heat transfer fluid (NREL, 2013*a*). In most cases this is either *Therminol® VP-1* or *Dowtherm® A* synthetic oils. These, however, limit the upper operating temperature to approximately 400 °C (Dow Chemical Company, 2001; Solutia Inc., 2013). Other disadvantages of the oils are degradation over time, high cost and inflammability. In the following, synthetic oils are not considered because their temperature limitations prevent high efficiency cycles.

## 3.2. Molten Salts

The first CSP pilot plants that used liquid salt as the HTF and thermal storage medium were the 1 $MW_e$ *Molten-Salt Electric Experiment* (*MSEE*), the 2.5 $MW_e$ *THEMIS* and the 10 $MW_e$ *Solar Two* central receiver power plants (Reilly and Kolb, 2001; Dunn et al., 2012). The operating temperature range of the latter was 290 °C to 565 °C with a binary salt, composed of 60 % of $NaNO_3$ and 40 % of $KNO_3$ (by mass) - so called **Solar Salt**™. Although *Solar Salt*™ is stable to higher temperatures of up to 600 °C, this lower maximum temperature has been chosen because its corrosion rate with the used stainless steel is acceptable at that temperature (Pacheco et al., 2000). The difference between the chosen lower temperature and the solidification temperature at 222 °C is to establish a safety margin for freezing.

The design steam parameters were 535 °C/100 bar in the 35 $MW_t$ steam-generator/-superheater unit and 510 °C/100 bar in the condenser turbine. The latter was refurbished from the *Solar One* predecessor and therefore a limiting factor in plant efficiency (Tyner et al., 1995; Pacheco et al., 2000). Pacheco et al. and Litwin (2002) summarized the results gained from tests and operation between 1996 and 1999. From these, Zavoico (2001) and Moore et al. (2010) deducted design options and standards for future central receiver (CR) molten salt power plants in great detail. On this basis, the next plant of this type was built - arguably the most advanced CSP plant to date: The 19.9 $MW_e$ *Solar Tres*/*Gemasolar* plant with 15 full-load hours of molten salt thermal energy storage (TES) (Lata et al., 2008). The latter enables 24 h power generation on summer days and, therefore, baseload capability. The nominal turbine inlet temperature generated in the steam generator is 542 °C (SIEMENS AG, 2010). Operating experience of the first year of power production of the plant are summarized by García and Calvo (2012).

Heat transfer characteristics of molten salts are mediocre. The reasonably high density and mediocre specific heat capacity enable a low volume flow but the low thermal conductivity leads to elevated temperatures on the outside of the receiver pipes and, therefore, high radiation losses. Rodríguez-Sanchez et al. (2013) investigated the influence of the number and diameter of receiver tubes in a *Gemasolar*-like plant on maximum tube temperature, maximum molten salt film temperature, HTF pressure drop and receiver cost (see Figure 1). The heat transfer between pipe and HTF can be improved by increasing the fluid velocity and turbulence (for example, by usage of spiral tubes as shown by Yang et al., 2010). Another way of improving a salt receiver's efficiency is to improve its optical efficiency, as done by Garbrecht et al. (2012) who built pyramid-like spikes in which the HTF circulates. The pyramids act as a trap for light and thermal radiation. The biggest advantage of molten salt as the HTF is the possibility of direct storage at relatively low costs.

**Advanced Molten Salts** The high solidification temperatures of liquid salts are problematic especially in line-focusing CSP plants (parabolic trough or linear Fresnel receivers) because the HTF would freeze during the night or in times of low irradiation. In CR plants, the salt will normally be drained into a tank while filling the receiver with gas. However, salt freezing, for instance, due to blocked valves, can still occur and

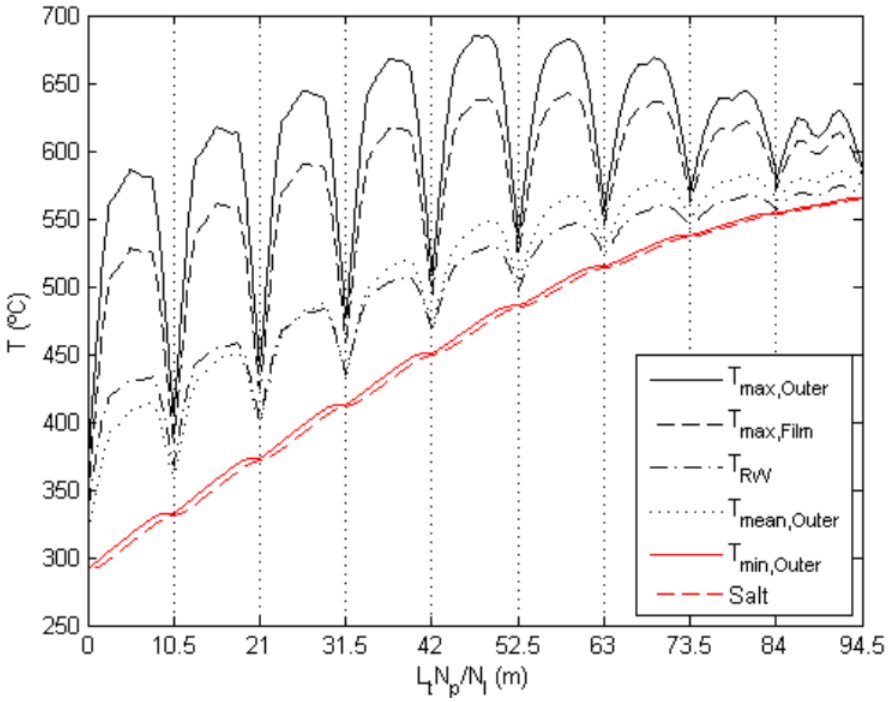


Figure 1: Temperatures over flow length through molten salt receiver ($L_t$: tube length; $N_l$: Number of lines in the receiver or salt paths; $N_p$: Number of panels in the receiver) (Rodríguez-Sanchez et al., 2013).

cause failures (Pacheco and Dunkin, 1996). Other possible solutions besides draining include trace heating or circulation of stored hot salts but all of these would result in higher heat losses, electrical power consumption and/or investment costs. To evade this complication, research is being done on liquid salts with lower melting points.

Raade and Padowitz (2011) reported the experimental finding of a quinary molten salt composition with a melting temperature as low as 65 °C and thermal stability above 500 °C. However, they state that the cost of the found salt "[...] is likely to be considerably higher than the simple binary Solar Salt [...]." Bauer et al. (2012) report the installation of a testing loop for degradation, stratification and corrosion testing of new salt compositions with melting temperatures as low as 75 °C and thermal stability comparable to *Solar Salt*™. They found enhanced thermal stability of the salts under oxygen enriched air. Siegel et al. (2011) measured the thermophysical properties of different low-melting-point molten salts.

Research is also currently being done on molten salts with higher maximum operating temperatures in order to allow higher efficiency power cycles (see for example, U.S. Department of Energy, 2012*a*). Kelly (2010) of *Abengoa Solar* wrote an extensive report on possible future implementation of supercritical Rankine cycles in CSP power plants. He discussed several scenarios at live steam temperatures of 565 °C, 590 °C and 650 °C (subcritical, supercritical and ultra-supercritical Rankine cycle, respectively) with dif-

ferent HTF/working fluid/TES combinations, two of which using molten salt as the HTF. Kolb (2011) estimated the economic benefits of raising the salt HTF's receiver exit temperature to approximately the same temperatures as investigated by Kelly and predicted levelized cost of electricity (LCOE) reductions of up to 8 %.

Raade et al. (2012) found a quinary composition of LiCl, NaCl, KCl, CsCl and $SrCl_2$ with a melting point of 253 °C at ambient pressure and thermal stability up to approximately 750 °C. The proposed maximum operating temperature of the so-called *Saltstream™ 700* is 700 °C. The novel salt consists of more than 70 % by weight of CsCl and LiCl, which are both expensive materials. The aim is to find compositions with reduced shares of these substances without considerable penalty on the thermal qualities.

Williams (2006) assessed different salts for use as coolants in next generation nuclear power plants. These allow for operation well above 700 °C at low pressure, however, they also mostly have high solidification temperatures (above 300 °C) and are substantially more expensive than, for example, *Solar Salt™*. Corrosion issues also have to be investigated for a lack of operating experience. Forsberg et al. (2007) proposed some of these salts for use in solar power towers with direct thermocline TESS and graphite as the filler material. The chosen power cycle in their model is a closed multi-reheat Brayton cycle with helium or nitrogen as the working fluid and operating temperatures between 700 °C and 1000 °C.

Olson et al. (2009) and Sabharwall et al. (2010) conducted experiments on a corrosion test loop at the *University of Wisconsin - Madison*. They heated up two different molten salts that could potentially be used in next generation nuclear power plants up to 500 °C, namely so-called *FLiNaK*, which consists of LiF-NaF-KF (46.5-11.5-42 mole percentage), and KCl-$MgCl_2$ (67-33 mole percentage), and observed the material loss of the following pipe materials over several hundreds of hours: *Hastelloy N, Hastelloy X, Inconel 617, Haynes 230* and *Incoloy 800H*. Sabharwall et al. found that the used graphite capsules greatly enhanced the corrosion rate. Because of this, the found values are much higher than in a graphite-free environment and shouldn't be used for deciding on an appropriate component material.

## 3.3. Liquid Metals

Other HTFs don't have the problematic upper and lower operating *T*emperature limitations of molten salt. For example, liquid metals and their alloys can have solidification temperatures below 0 °C and boiling temperatures above 1600 °C. Freezing of the HTF inside pipes, the receiver, valves and TESS can, therefore, practically be eliminated. At the same time, the HTF can operate at low pressures and still reach the temperatures required for a next-generation Rankine or a Brayton power cycle.

Another upside of liquid metals are the outstanding heat transfer characteristics and the low viscosity. Due to the high thermal conductivity, the temperature gradient of the flow inside the receiver pipe will be very small. Additionally, the pipe thickness can be kept small as well because of the low pressure. This leads to maximum pipe temperatures close to the fluid's exit temperatures (Boerema et al., 2012) - resulting in higher receiver efficiencies - and reduced strain inside the pipe caused by thermal

expansion (Lata et al., 2008). Eventually, these properties allow higher maximum solar fluxes on the receiver and, thus, a higher thermal efficiency of it. Kelly (2010) stated the maximum allowable incident flux on a molten salt receiver (20 bar inside pressure, 696 °C maximum outer pipe temperature) to be as high as 2.5 $MW_t$. This is notably higher than fluxes in realized projects, which, according to Lata et al., are 0.8 $MW_t$ for *Solar Two* and 1.0 $MW_t$ for *Gemasolar*. Liquid metal receivers can tolerate even higher influxes.

Pacio and Wetzel (2013) assessed different types of liquid metals as HTFs for CRSs. They investigated sodium, the eutectic lead bismuth composition and tin as candidate materials and stated their advantages, limitations and areas of recommended future research.

### 3.3.1. Sodium

So far, the focus in liquid metal HTF research was on sodium. In the 1980s' *Small Solar Power Systems Project of the International Energy Agency* (IEA-SSPS), a sodium-cooled external receiver was tested at the Plataforma Solar de Almería (Schiel and Geyer, 1988). Its nominal incoming power was 2.7 $MW_t$ at a maximum fluid temperature of 560 °C and a maximum heat flux of 1.4 $MW_t/m^2$. However, the tube receiver was also tested at a radiation input of up to 3.4 $MW_t$ with a heat flux of up to 2.5 $MW_t/m^2$, producing pipe temperatures up to 770 °C. Post-experimental metallurgical analyses didn't show any significant deformations or creep damage of the pipes even under these super-nominal conditions.

Boerema et al. (2011) showed with a high-level comparison of *HITEC® Heat Transfer Salt* and sodium as HTFs for CR plants, that the main advantage of the latter (besides the higher operating temperature) is the lower pipe temperatures due to the high thermal conductivity. This enables higher radiation fluxes (as mentioned above), smaller aperture areas and, therefore, lower heat losses (see Figure 2). However, the heliostat field has to be able to focus on this smaller target and stresses on the pipes are potentially higher.

A big concern with the use of sodium as an HTF is the strong exothermic reaction with water in which hydrogen is one of the products. In 1986, the IEA-SSPS project ended in a sodium fire, destroying some of the equipment. The International Atomic Energy Agency (1999) reported the fire was a sodium spray fire that resulted in sodium spillage of approximately 10 000 kg and burned at 225 °C, while An (2011) and Boerema et al. (2012) mentioned 14 000 kg of leakage and a maximum flame temperature of 1200 °C. The incident was caused by maintenance procedures on a valve. This event stopped most research on sodium in CSP but the nuclear industry has continued working on sodium as a nuclear reactor coolant (for example, Poplavskii et al., 2004). Guidez et al. (2008) stated that the combined reactor time of sodium-cooled plants exceeds 388 years with mostly promising experiences gained. However, there have been sodium leaks and often fires in almost all reactors that ever went critical (Poplavskii et al., 2004).

Recently, liquid metals, including sodium, have been investigated as HTFs for CSP plants again (Singer et al., 2010; Kotzé, Backström and Erens, 2012*b*; Boerema et al., 2012; U.S. Department of Energy, 2012*b*; Hering et al., 2012; Pacio and Wetzel, 2013).

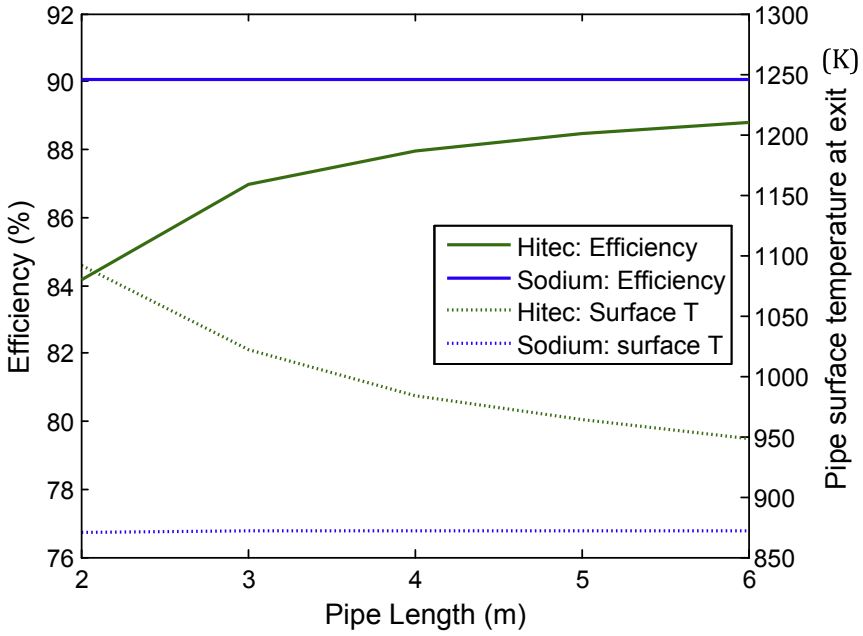


Figure 2: *HITEC® Heat Transfer Salt* and sodium receiver efficiencies and maximum surface temperatures for various pipe lengths. Emissivity = 0.85, concentration ratio = 1300, $D = 9\,\text{mm}$ (Boerema et al., 2012).

Hering et al. described the possible direct conversion of the heat in the sodium to electric power in an alkali metal thermal electric converter (AMTEC) cycle. The possible use of magnetohydrodynamic (MHD) pumps for sodium could be of merit because of their low maintenance requirements. The AMTEC technology is not available for the given parameters yet.

### 3.3.2. NaK

The eutectic sodium-potassium alloy NaK78 (22.2-77.8 mass percentage) melts at ambient pressure at $-12.6\,^{\circ}\text{C}$ and boils at $785\,^{\circ}\text{C}$ (Foust, 1972). Despite the inferior heat transfer characteristics of NaK78 as compared to sodium, the low solidification point makes it very attractive for transient power plants, like CSP. Freezing issues in pipes, vents and the receiver are practically eliminated. Other non-eutectic NaK alloys could show more favorable thermodynamic properties for plants, like higher densities, at the cost of higher solidification temperatures (see Kotzé, Backström and Erens, 2012*b*). Otherwise, the characteristics of and issues with NaK are very similar to those of pure sodium and can be found in the elaborate handbook by Foust.

Diver et al. (1990) presented the state of the art in parabolic dish CSP systems at the beginning of the 1990s. They focus on indirectly heated Stirling engines with liquid metal HTF that are evaporated in the receiver and condense on the heat exchanger to the engine. They mention sodium, potassium and NaK78 as investigated and tested

HTFs, depending on temperature limits in the receiver.

### 3.3.3. LBE

Another liquid metal alloy investigated for CSP applications is the lead bismuth eutectic composition Pb-Bi (44.5-55.5) (LBE). According to Pacio and Wetzel (2013), it does not have the problematic drawback of sodium or NaK (reaction with water) and has a very high density, leading to much lower flow speed requirements. The boiling temperature of LBE (1670 °C) is even higher than that of sodium but the solidification temperature (125 °C) is higher as well, so that freezing is an issue. Additionally, the high corrosivity and cost of LBE could be problematic (Furukawa et al., 2004; Zhang and Li, 2008; Pacio and Wetzel, 2013).

### 3.3.4. Summary Liquid Metals

Liquid Metals have very high potential as HTFs because of their wide range of practical operating temperatures and the superior heat transfer characteristics. They allow for high maximum fluid temperatures at low pressures, high receiver efficiencies and low pressure drops. However, they don't qualify as a direct storage medium due to their high costs and are challenging in terms of operation, maintenance, safety and steel corrosion.

## 3.4. Liquid Glasses

Glasses are known to be chemically stable and withstand high temperatures. However, they have high melting temperatures and high viscosities even at elevated temperatures so that pumping becomes problematic. Halotechnics (2013) introduced **Haloglass™ RX**, a glass which is pumpable down to 450 °C and has some properties that would qualify it as an HTF. Due to the high minimum operating temperature it is not promoted here but instead presented as a possible high-temperature storage medium in Section 9.4 with some more properties given in APPENDIX B.1.1.

# 4. Gases

The upper temperatures of gaseous HTFs in CSP systems are usually only limited by the materials of the receiver pipes, ducts, etc. They are therefore especially suited for high-temperature applications. Gases, however, have the downside of low heat transfer coefficients and densities.

Gases can be used to directly power a gas turbine, thus making use of the very high temperatures which can be generated in a CR. The exhaust gases can be used to power a bottoming (Rankine) cycle, which renders possible high thermal system efficiencies.

## 4.1. Air

Air is the obvious choice as the HTF of a Brayton cycle. It is available everywhere, non-hazardous, theoretically free of cost and does not necessitate a heat exchanger for co-firing. On the other hand, it has a low density and unfavorable heat transfer characteristics and therefore makes big heat exchangers and receivers necessary. For the implementation of a CSP receiver in a gas turbine (GT), it has to be **pressurized**. The pressure drop has to be paid special attention to because the GT's performance is highly dependent on the pressure drop in between compressor and expander.

Receivers are the crucial element of CSP plants with air as the HTF. Due to the difficult heat transfer characteristics, effort has to be made to reduce the aperture area and temperature differences between the receiver and the fluid.

In the *SOLGATE* project, several institutes and companies (including the DLR[1] and CIEMAT[2]) developed and tested a 250 $kW_e$ CR CSP prototype at the Plataforma Solar de Almería (EC, 2005). It consisted of three air-cooled receiver modules connected in series. The low temperature (LT), intermediate temperature (IT) and high temperature (HT) receiver modules heated up the pressurized air approximately from 300 °C to 550 °C, to 730 °C and to 960 °C, respectively. The nominal expander inlet temperature of the GT was raised to about 1200 °C by a gas combustor. This co-firing enhanced the GT efficiency while decreasing the solar share of the thermal energy input.

The *SOLHYCO* project was the successor of *SOLGATE*. It featured a 100 $kW_e$ microturbine with recuperator and a combustor for bio-diesel (DLR, 2010). The recuperator noticeably increases the inlet temperature into the receiver and, therefore, enables a single high-temperature receiver instead of the threefold receiver system in *SOLGATE*. The HT receiver was changed considerably from a pressurized volumetric to a pressurized tube design featuring novel *profiled multilayer* (PML) tubes. These address two problems that lead to high temperature differences between the outside of the pipe and the final receiver outlet temperature: a) the high temperature gradient between irradiated and non-irradiated side of the tubes is decreased by introducing a layer of copper in between two thin concentric steel pipes, which increases the thermal conductivity of the resulting pipe; and b) the heat transfer to the air flow is increased by adding a wire-coil structure to the inner pipe wall (see Figure 3). The PML tubes were not installed into the final receiver because of manufacturing delays, however, laboratory tests with them showed the expected homogenization of the tube temperatures. For the use in a commercial power plant, some issues with the intermetallic connection's durability would have to be resolved. The maximum receiver outlet temperature reached was approximately 800 °C. Several design flaws, that limited this temperature and the receiver efficiency, could be identified and solutions proposed.

The next stage in the development of a solar combined cycle power plant was the increase of the size to a demonstration plant with a 4.6 $MW_e$ industrial gas turbine (without bottoming cycle). The Solugas Consortium (2012) consists of *Abengoa Solar*, the *DLR*, *GEA*, *Turbomach* and *New Energy Algeria*. The start-up tests of the plant

[1] DLR: German Aerospace Center
[2] CIEMAT: Center for Energy, Environment and Technological Research

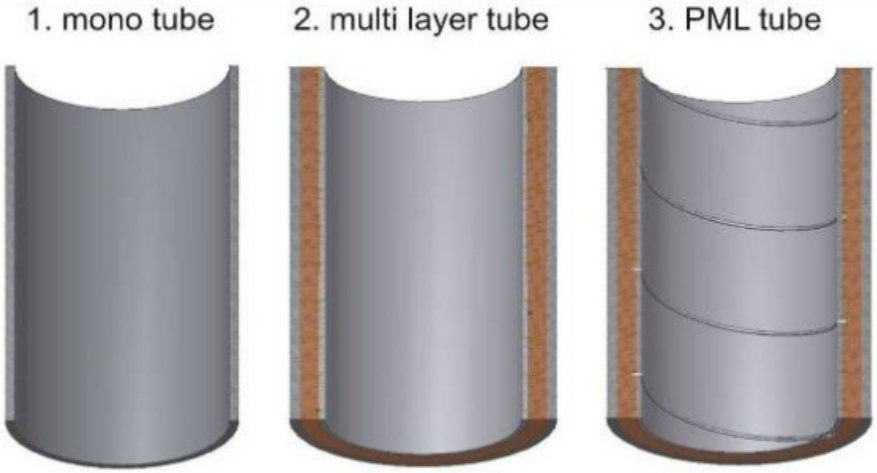


Figure 3: Visualization of different tube designs (EC, 2005).

were commenced in May 2012 but no detailed information could be retrieved.

Schwarzbözl et al. (2006) economically analyzed different designs for hybridized solar gas turbine prototype systems between 1 $MW_e$ and 15 $MW_e$ for two different locations. They found LCOE values for solar-generated energy between 0.13 EUR/kW $h_e$ and 0.90 EUR/kW $h_e$ depending on unit size and solar share.

Other receiver designs were proposed, for example, a pressurized closed volumetric receiver by Hischier et al. (2009), an irradiated ceramic plate heat exchanger by Jensch et al. (2012) and others, as summarized by Ávila Marín (2011). An Israeli Company, Aora Solar Ltd (2012), makes use of a solar-driven microturbine to generate off-grid power and heat (with considerable co-firing of natural gas).

Air can also be used as an HTF without being the working fluid. In this case the hot air can drive, for example, a Rankine steam cycle through a heat exchanger. For this application, an **open air receiver** is usually used for simplicity reasons. The air doesn't have to be pressurized (except to overcome pressure drops in receiver, piping and heat exchanger) and the turbine is not directly coupled with the receiver outlet flow. However, the advantage of using a high temperature working fluid can not be made use of, since Rankine cycles are today limited to approximately 640 °C. The only commissioned demonstration plant using this technology for grid-power is the *Jülich Power Tower*, as described by Hennecke et al. (2009). In the *AlSol* project, this technology is planned to be used in a 7.1 $MW_e$ hybridized solar-natural gas power tower (Koll et al., 2011).

Wilson Solarpower (2010*a*) proposed a system in which unpressurized air is used as the HTF in a closed receiver. This hot air then heats pressurized air in a regenerative heat exchanger (see Figure 4) to be used in the microturbine of a Brayton cycle.

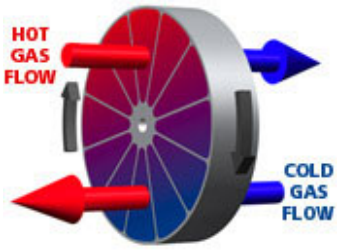


Figure 4: Regenerative air-air heat exchanger (Wilson Solarpower, 2010*b*).

### 4.2. Other Gases

Other Gases, like helium, $CO_2$ or nitrogen could also be used as HTFs for their superior heat transfer and flow characteristics or material compatibility (corrosion) as compared to air (Becker, 1980). Massidda and Varone (2007), for example, analyzed heat transfer, pipe stresses and pressure drops for helium as the HTF in absorber tubes. They also investigated heat transfer enhancing measures, like swirl tapes or increased pipe roughness. All of these gases have specific problems and are far from the demonstration phase.

### 4.3. Summary Gaseous HTFs

Air is by far the most investigated gaseous HTF. This is because of its practically infinite availability and extensive experience with it as a heat transfer and working fluid. The high operating temperatures of the fluid enable combined cycle plants with high efficiencies, however, the heat transfer poses a problem due to the HTFs' low density and thermal conductivity.

## 5. Solids

### 5.1. Particle Receiver

Wu et al. (2011) compared three different direct absorption receivers (DARs), two of which were open particle receivers. In DARs the heat is directly absorbed in the form of radiation by the HTF (see Figure 5) instead of being transferred through, for example, steal pipes in the form of conduction and then being transferred to the HTF via convection. The maximum receiver temperature can, therefore, be found in the HTF and not on the receiver material which leads to decreased radiation losses and material stress. Open particle receivers feature solid particles surrounded by a fluid. This can have several advantages, for example, increased radiation absorption, higher heat capacity or lower material temperatures towards the surroundings.

Chen et al. (2007) developed a computational fluid dynamics (CFD) model of an open particle receiver in form of a curtain of ceramic particles between 200 µm and 600 µm in size. Their simulations show good agreement with experimental results. The calculated

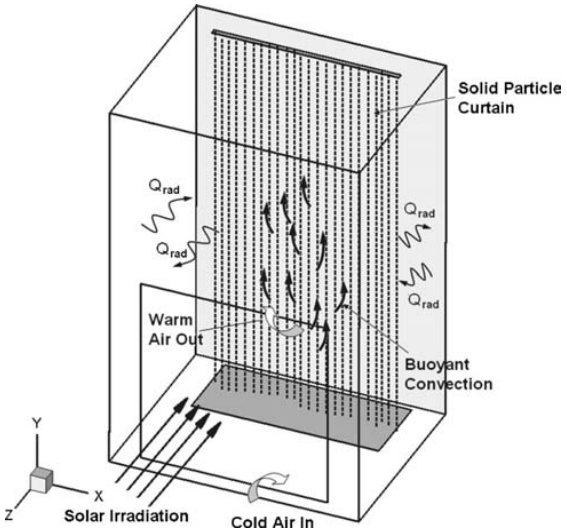


Fig. 1 Schematic illustration of aerodynamic and thermal processes in a solid-particle receiver

Figure 5: Schematic illustration of aerodynamic and thermal processes in a solid-particle receiver (Chen et al., 2007).

receiver efficiencies for the small and simple receiver are below 70 % for particle outlet temperatures of less than 1000 K.

Crocker and Miller (2011) modeled a cylindrical volumetric receiver with air and carbon nano particles as the HTF. Their initial CFD simulations suggest fluid outlet temperatures of up to 1430 K but many questions of the design weren't answered at the early stage of the research.

Thermal efficiencies of solar particle receivers are expected to reach 90 % (Ho, 2010). However, they are still in an experimental stage and several questions, for example, the heat transfer to the working fluid, are to be answered.

# 6. Fluids with Phase Change

## 6.1. Direct Steam Generation (DSG)

The direct generation of steam inside the receiver (DSG) has been the subject to research and development for a long time. The *Solar One* tower as well as the first two commercial power tower plants, *PS10* and *PS20* with a power rating of 10 $MW_e$ and 20 $MW_e$ use(d) saturated steam as the HTF (NREL, 2013*a*). The latter both produce steam at 40 bar and 45 bar, respectively, at an outlet temperature below 300 °C and have been running for several years.

The first two-large scale linear Fresnel solar power plants, *PE1* (1.4 $MW_e$) and *PE2* (30 $MW_e$), rely on the same HTF but evaporate the water in a line focusing system (Novatec Solar, 2013). In nominal conditions, the steam in the receiver pipes is heated

to 270 °C at a pressure of 55 bar, however, temperatures above 500 °C have been achieved during tests in the *PE1* plant.

DSG is difficult to realize in parabolic trough power plants because of the relatively high pressures necessary and the resulting stresses on joints. However, numerous studies investigated the technology and see high potential for cost reduction and efficiency increase. These have been summarized by Birnbaum et al. (2008). Due to the two-phase flow inside the pipes, the heat transfer is difficult to exactly measure or predict. Therefore, more water is added to the evaporator to ensure sufficient heat transfer and a water-steam-separator has to be incorporated to protect the turbine from high moisture content (Mertins, 2009).

Eck and Zarza (2006) compared saturated with superheated steam parabolic trough DSG plants' performances. They found that the benefits in power block efficiency of a superheated plant is often compensated for by the higher thermal receiver losses. The decision for one of the two designs has to be made under consideration of part-load behavior, TES implementation and cost (investment as well as operation and maintenance).

Feldhoff et al. (2012) compared different steam generation modes in parabolic trough DSG plants and further investigated the once through method.

The TES poses a big problem in DSG plants. Because of the incorporation of preheating, evaporation and superheating, a combination of sensible heat and a latent heat TES seems most viable. Due to the temperature gradient between HTF and the latent TES, the steam pressure during storage discharge has to be significantly lower than when the turbine is fed directly from the solar field (Birnbaum et al., 2008). More information on the implementation of TESs in DSG plants can be found in Section 13.

# 7. Supercritical Fluids

## 7.1. s-$H_2O$

Supercritical water (s-$H_2O$, $p_{\mathrm{crit},H_20} = 221$ bar) has been used as a working fluid in conventional power plants for decades. The state of the art are so called 'Ultra-Supercritical' (USC) steam plants with parameters of up to 620 °C/310 bar (Boss et al., 2007). USC turbines are usually installed in big coal power plants, their ratings range between approximately 200 $MW_e$ and 1050 $MW_e$ and the plants reach net efficiencies in excess of 45 %. Next generation advanced USC (A-USC) plants are expected to run at turbine inlet temperatures of between 700 °C and 760 °C (Weitzel, 2011) with efficiencies above 50 %.

Due to the high critical pressure of water, s-$H_2O$ requires special - usually expensive - materials for piping, turbomachinery and heat exchangers. No solar power plant using s-$H_2O$ as the HTF has been built so far. However, Coventry and Pye (2010) proposed a parabolic dish system, employing s-$H_2O$ or superheated (subcritical) water as the HTF and working fluid with a molten salt system as the storage. The advantage of s-$H_2O$ is the lack of the evaporation process which leads to smoother isobaric heating processes as compared to superheated fluids. The heat transfer between the fluid and another

single phase fluid (for example, molten salt) is, therefore, exergetically preferrable (see Figure 6). Coventry and Pye found a slightly higher overall efficiency for their USC cycle as compared to the superheated cycle. However, the outcome highly depends on system parameters and assumptions.

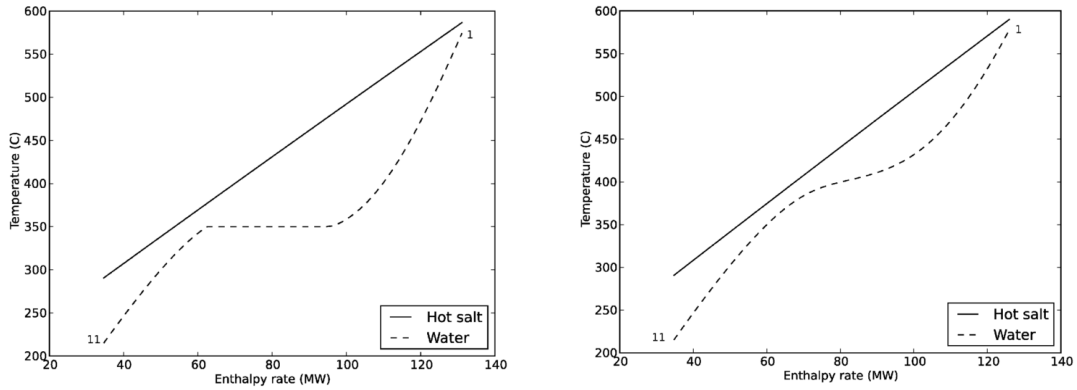


Figure 6: Subcritical and supercritical heat transfer in systems with one HTF (Coventry and Pye, 2010).

## 7.2. s-$CO_2$

Compared to water, carbon dioxide has a much lower critical pressure of 73 bar, yet supercritical $CO_2$ (s-$CO_2$) is relatively dense at approximately 0.6 kg/m$^3$ (Wright, Conboy and Rochau, 2011). On the one hand, these characteristics decrease stresses on pipes and flow speeds, on the other hand, turbomachinery and heat exchangers at a fraction of the size of steam components can be realized. Turchi (2009) gave an introduction to s-$CO_2$ as an HTF and/or working fluid in CSP plants and listed (dis-)advantages when compared to other candidate HTFs. Gary et al. (2011) presented an s-$CO_2$ combined cycle solar power tower with a LCOE of 0.06 USD/kW $h_e$ as one of the targets for 2020 in the *SunShot* initiative.

*Sandia National Laboratories* have done extensive research on s-$CO_2$ cycles for several different applications (solar, geothermal, nuclear) and summarized the testing and development outcome in (Wright, Conboy, Parma, Tom G. Lewis, Gary A. Rochau and Ahti J. Suo-Anttila, 2011) and (Wright, Conboy and Rochau, 2011). They proposed cycles in the small to medium range (0.1–10 $MW_e$), for instance, in modular CR systems.

Chapman and Arias (2009) compared three parabolic trough configurations with synthetic oil, subcritical $CO_2$ and s-$CO_2$ as HTFs, respectively. They found that the pumping work for subcritical loops would be orders of magnitude higher than in the base case (oil). Thanks to its higher density, s-$CO_2$ is much more favorable in that sense. However, the high pressure dramatically increases the requirements on pipes and will most likely not be feasible in line-focus systems but only in CR systems.

Chapman and Arias (2009) as well as Ma and Turchi (2011) addressed the problem of adding a TESS to a s-$CO_2$ system. The latter proposed molten salt as the storage

medium, however, this would limit the turbine inlet temperature (at least during discharging) to much less than 600 °C. Active direct and passive storage systems appear not viable due to the need for high pressure tanks.

Cox (2009) found that standard heat transfer correlations are in general applicable to s-$CO_2$ heat exchangers. However, in close proximity to the critical point the measured heat transfer noticeably differed from the calculated values.

Rouillard et al. (2009) compared the corrosion effects on a ferritic-martensitic and different austenitic steels in contact with s-$CO_2$ at a temperature of 550 °C and a pressure of 250 bar. Their research was aimed at the development of components for the secondary cycle for advanced (for example, sodium-cooled) nuclear reactors. It turned out that corrosion had a much more profound effect on ferritic-martensitic steels as compared to austenitic ones.

**Characteristics as Working Fluid** Dostal et al. (2004) gave an elaborate overview on s-$CO_2$ as a working fluid and possibly HTF in nuclear power plants. The information found in their report is also applicable to CSP, as they investigate different configurations, for example, with liquid metal cooled reactors and s-$CO_2$ only as the working fluid. In this design, one advantage in terms of safety is that there is no direct heat exchanger between liquid metal and a water/steam cycle. $CO_2$ also reacts exothermally with liquid metals but no hydrogen is created in the reaction, therefore greatly decreasing the hazards associated with liquid metals. Dostal et al. built a model for different s-$CO_2$ cycles - some of them with preheating, reheating, precooling or intercooling - and compared them with each other and to a supercritical water and an ideal gas Brayton cycle with helium as the working fluid. With this model, they investigated the influence of heat exchanger (precooler, regenerator, etc.) sizes on thermal efficiency and pressure losses. In general, they see great potential in s-$CO_2$ cycles due to the simple layout of Brayton cycles as compared to Rankine cycles and the high efficiencies at moderate pressures/temperatures. The latter is caused by the cycles' low compression work due to the low compressibility factor of $CO_2$ at the critical point. Mentioned problems are little experience in compressors that work in close proximity of the critical point, higher corrosion rates than those of helium and recuperators for real gases (pinch-point problem).

Kato et al. (2004) investigated the implications of precooling and intercooling in $CO_2$ power cycles at pressure levels of 70 bar and 125 bar for nuclear reactors with a fluid outlet temperature of 800 °C. In their model, certain configurations of compressor stages and a bypass compressor improved cycle efficiency by up to 6 percentage points.

Muto and Kato (2007) compared s-$CO_2$ cycles at different temperatures (500–650 °C), pressures (80–200 bar) and with single or dual expansion for next generation nuclear reactors in the power rating range of 200 $MW_e$ to 600 $MW_e$. The found efficiencies varied between 42.6 % and 50.3 % for the designs with different recuperation concepts. The dual turbine layout allows for a potentially beneficial concept: The highest temperature is produced in the low pressure turbine stage and its outlet temperature is still higher than the inlet temperature to the high pressure stage. The whole heating process for the high pressure side can, therefore, be achieved by an internal recuperating heat exchanger (see

Figure 7). The heat source (reactor/solar receiver/etc.) does not get in contact with the high pressure fluid, which reduces stresses on the heat generating component.

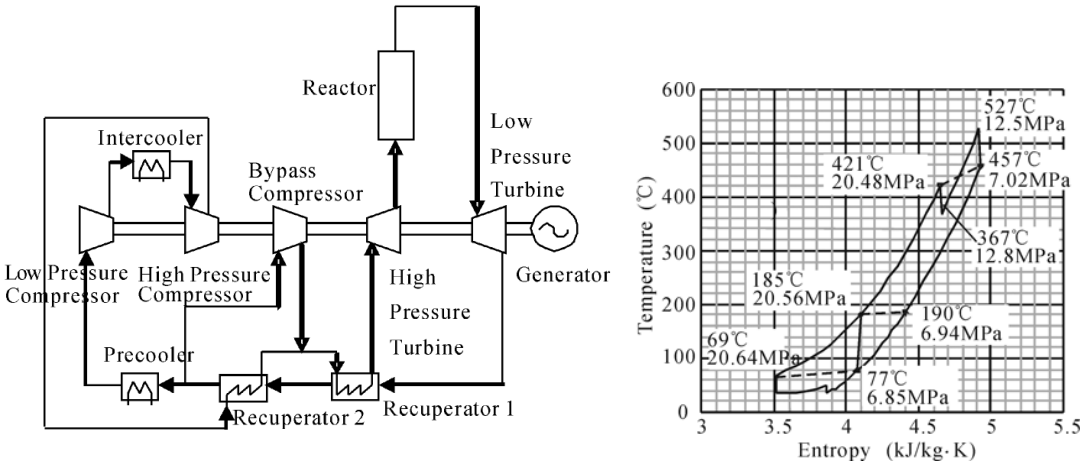


Figure 7: Scheme and T-s diagramm of dual-expansion s-$CO_2$ power cycle (Muto and Kato, 2007)

Another thermodynamic comparison of $CO_2$ cycles was conducted by Kulhánek and Dostál (2011). They investigated four different designs — namely the simple Brayton, precompression, recompression and the partial cooling cycle — at turbine inlet temperatures of 500 °C to 850 °C. They found that the partial cooling cycle provides the best efficiencies, however, at the cost of a more complex design with three compressor units. At high temperatures, the precompression cycle is the second most efficient and it appears to have favorable part-load properties.

Moisseytsev and Sienicki (2010) conducted s-$CO_2$ power cycle simulations for the *Very High Temperature Reactor* (VHTR) concept. This type of nuclear reactor is cooled by helium, which is heated from 400 °C to 850 °C in the core, producing approximately 600 $MW_t$. The high temperature difference poses problems on an s-$CO_2$ power cycle because the optimal value for turbines operating between 200 bar and 75 bar is only 150 K. Moisseytsev and Sienicki analyzed several solutions to efficiently couple the two cycles. The first one is a cascaded system of three single cycles (Figure 8) with the optimal specifications stated above. They each have the same heat input of 200 $MW_t$ but their efficiencies vary in a wide range with values of 54 %, 50 % and 44 %, respectively.

To avoid a high number of turbomachinery and heat exchangers, the optimal temperature difference of a s-$CO_2$ cycle can be increased by increasing the turbine pressure ratio. Since increasing the cycle's maximum pressure creates material problems, a decrease in the turbine outlet pressure seems more feasible. However, a large portion of the efficiency advantages of a s-$CO_2$ cycle is created by compression close to the critical point. Therefore, a cycle with one or two subcritical pre-compression stages and pre-coolers

was analyzed. The latter (see Figure 9) has a turbine outlet pressure of approximately 11 bar, increasing the temperature difference in the cycle to 430 K. The resulting overall cycle efficiency (50 %) is higher than that of the cascaded cycle (45 %) while having simplified the cycle considerably.

**Summary s-$CO_2$** Supercritical $CO_2$ cycles show higher efficiencies than state of the art steam or air cycles. Other benefits are a higher density, much smaller machinery, simpler plant design and a lower supercritical pressure. These don't only apply to CSP plants and much research has been done to promote s-$CO_2$ as a working fluid/HTF in next generation nuclear and conventional power plants as well as for cooling applications. However, considerable effort is still necessary to develop components for utility scale power ratings (Fuller and Batton, 2009; Sienicki et al., 2011). One of the programs financed by the *SunShot* initiative is the development of a 10 $MW_e$ s-$CO_2$ turbine for application in CSP plants at *Sandia National Laboratories*.

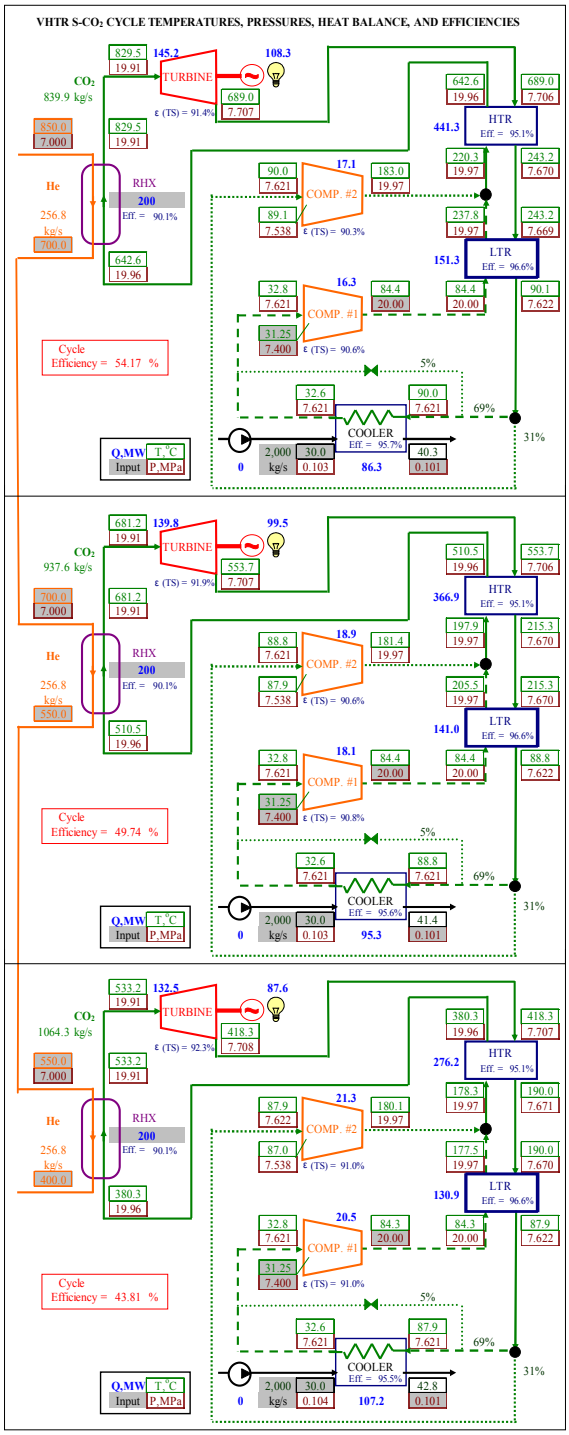


Figure 8: Cascaded s-$CO_2$ power cycle (Moisseytsev and Sienicki, 2010)

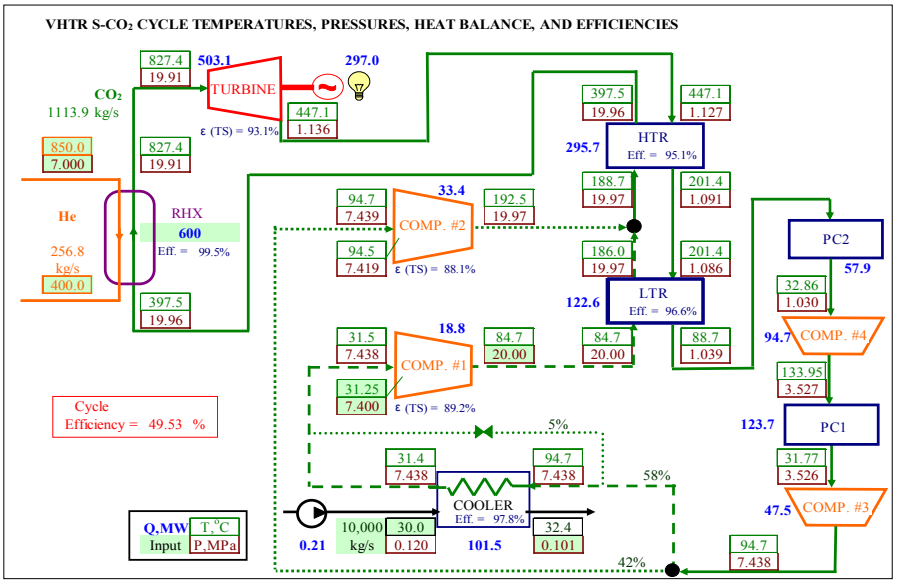


Figure 9: s-$CO_2$ power cycle with two precoolers (Moisseytsev and Sienicki, 2010)

# Part II.
# Thermal Energy Storage Systems

## 8. Introduction

In CSP plants, thermal energy storage systems (TESS) serve multiple purposes. They balance the plant in transient periods, for example, during overcast, they enable stable turbine conditions and more full-load hours. The most important reason for the implementation of big TESS is, however, to be able to supply dispatchable or base-load power to the grid and even stabilize it on demand. This also increases the capacity factor of the power block and minimizes defocusing of mirrors.

This section gives an overview of the available types of TESS for CSP applications and their characteristics. Alternative introductions to TESS concepts, storage media and their heat transfer characteristics can be found in the literature (for example, Cabeza et al., 2012; Gil et al., 2010; Medrano et al., 2010; Li et al., 2011). The letter also describes the modeling of TESSs. As summarized by Duffie and Beckman (1991) and Gil et al., the major requirements on TESSs for CSP are:

- (volumetric) energy capacity
- charge and discharge heat rates
- maximum and minimum temperatures, sensible or latent heat storage

- safety and environmental impact
- thermal and chemical stability for thousands of cycles in contact with different materials
- heat losses
- quality of the thermocline after charging
- degradation of the thermocline during idle mode
- power requirements for charge and discharge
- costs (for the whole storage *system*)

NREL (2013*a*) shows which TES systems have been and are being built into CSP plants. The simplest way of storing heat in a CSP plant is to use the primary HTF as the storage medium as well, a so-called **active direct** storage system (see Figure 10(a)). This works well when synthetic oil (as in Luz Industry's *SEGS*[3] I plant) or molten salts (as in the *Gemasolar* plant) are used because they remain liquid at elevated temperatures but the high price, especially of synthetic oil, proves a big financial drawback. In DSG plants or when gas is the primary HTF, either a gaseous medium would have to be stored, resulting in low volumetric energy capacities, or a high pressure inside the tank is necessary to condense the medium, which makes long-time storage nonviable.

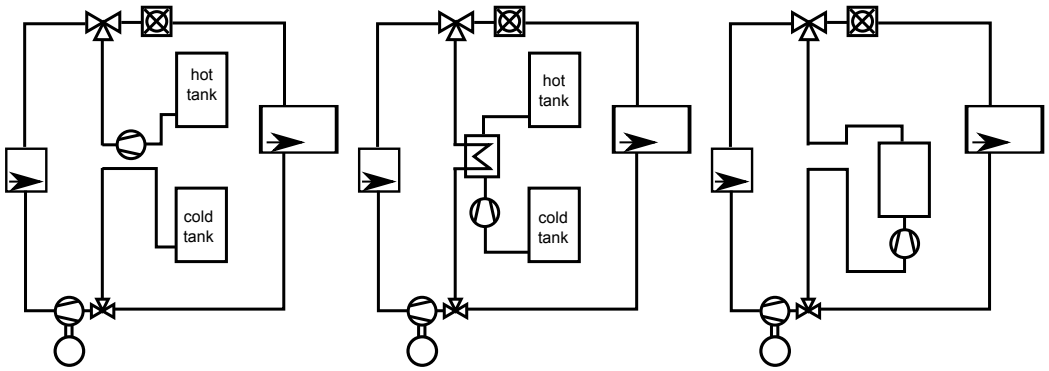


Figure 10: TESS types: (a) active direct, (b) active indirect, (c) passive

In **active indirect** storage systems (see Figure 10(b)), the storage medium is separated from the primary HTF by a heat exchanger. The advantage of this configuration is that no compromises have to be made in finding a medium that serves as both, an HTF and the storage medium. Instead two 'specialized' media can be used. The trade-off is between the avoided losses in the heat transfer/component cost reduction on the one hand and media cost reduction/efficiency improvement through the use of optimized media on the other hand.

[3]SEGS: Solar Energy Generation System

So far, commercial TESSs are all of the active two-tank type, with approximately the volume of storage medium in the system to fill one of them. One attempt to lower the cost of TESSs is to omit one tank and use one-tank for the hot and the cold storage medium. The separation between the states can be achieved, for example, by use of a moving separation disk (see Hering et al., 2012) or **thermocline** separation due to density differences in the medium. Thermocline systems can be fitted with solid so-called "filler material" with high thermal capacity. Compared to active one-tank systems, filler material can enhance the overall capacity, improve the thermocline quality and save costs by substituting an expensive fluid storage medium with cheaper solid particles, for example, ceramics or rocks. Storage systems in which the filler material material is the main contributor to the capacity are also referred to as '**passive**' (see Figure 10(c)). Depending on the used solid material and HTF, the materials can be in direct contact or separated (for example, by pipes, meshes or capsules around the storage medium to avoid chemical/mechanical interactions or improve heat conductivity).

**Forms of Storing Thermal Energy** According to Gil et al. (2010), thermal energy can be stored in three different forms: as a temperature rise (sensible heat), a phase change (latent heat) or chemical potential. Chemical and phase change material (PCM) storage systems promise great opportunities but are still subject to research whereas all existing TESS of CSP plants store sensible heat.

**Previous Reviews** Pilkington Solar International GmbH (2000) and Herrmann and Kearney (2002) gave elaborate overviews of storage systems and media investigated and built in the 1980s and 90s and some information on promising PCMs and solid media for passive TESS. Gil et al. (2010) gave an updated review on TESS for CSP applications. Kelly (2010) investigated the technical feasibility and economic viability of 5 concepts for future CR systems with supercritical working fluids including storage concepts (some of them with a separate low-pressure salt HTF). Reviews and screenings mainly of PCMs for high temperature applications have been conducted by Hoshi et al. (2005), Kenisarin (2010), Fan and Khodadadi (2011) and Liu et al. (2012). Some properties of the materials, that were decided to be appropriate for high-temperature storage ($> 550\,°C$), can be found in APPENDIX B.1 and B.2.

# 9. Media for Active Sensible Heat TESSs

## 9.1. Storage Media in Use

The first two *SEGS* plants featured a direct TESS with oil as the storage medium. Because of the high cost of the storage medium/HTF, this system has not been build since. All other commercial TESSs are based on *Solar Salt*™ as the storage medium.

## 9.2. Molten Salts

**Solar Salt**™ (see also Section 3.2) is liquid at ambient pressures between 220 °C and 600 °C which meets the requirements of today's superheated steam power cycles well. The volumetric heat capacity in this temperature range is good and the specific cost of the medium is relatively low (see APPENDIX A.3), however, for state of the art high-efficiency supercritical steam or Brayton cycles, the upper temperature poses a limitation. Additionally, the high melting temperature means that at least the pipes and valves of the TESS have to be taken care of in terms of freeze blockage, storage tank insulation has proven efficient against thermal losses and mechanical stresses. Corrosion of pipes and the tank system can be controlled at a tolerable level (see Kolb, 2011). Experiences of the first commercial-plant-sized salt TESS are summarized in Reilly and Kolb (2001). Querol et al. (2012) reported on the construction and tests of a demonstration single-tank active direct TESS with a floating barrier separator between hot and cold part. The 24 MW $h_t$ tank has been installed at the *Valle2* parabolic trough plant.

To sum up, *Solar Salt*™ is a good storage medium in many ways. The biggest drawback is the upper temperature limit which prohibits higher power cycle efficiencies. The relatively high melting temperature makes freeze protection necessary which, however, mainly influences its use as an HTF. The effect of this is that it has not been used in active direct TESS for line-focusing CSP application. The medium's cost is low but, due to the large amounts of storage medium necessary, plays a big role in CSP plants' total cost. Therefore, other media, even if only slightly cheaper, have to be investigated.

Alternative high-temperature or low-melting-point salts (see Section 3.2) are assumed to, at least in the medium term, have much higher specific costs than *Solar Salt*™. Even if they are used as an HTF, they will likely not be used as the (sole) storage medium.

Cordaro et al. (2011) presented the results of their measurements of different thermodynamic properties of several salts and mixtures that are thought to have potential as TES media. Their measurements show non-linear mixing behavior for properties of some of the mixtures, that differ from prior literature.

Zhao and Wu (2011) investigated **ternary salt compositions** consisting of $KNO_3$, $LiNO_3$ and $Ca(NO_3)_2$. Some of the reported solidification temperatures were below 100 °C, the compositions were stable above 400 °C and the costs were only slightly higher than those of *Solar Salt*™. The focus of Zhao and Wu was on line-focusing CSP technology as can be seen from the relatively low temperature stability limit.

## 9.3. Sodium

Because of its lower density and much higher price as compared to *Solar Salt*™, sodium is not viable as a storage medium in the temperature range *Solar Salt*™ operates in. According to Boerema et al. (2012), the fluid cost and storage volume for sodium as compared to *Solar Salt*™ will be 3.2 and 1.8 times higher, respectively. Only when sodium is used as the HTF and storage medium in a direct configuration or when the higher temperatures are utilized, does its use appear attractive. When technical challenges of sodium, for example, reactivity with water and possibly corrosion, have been overcome,

life-time optimizations of a CSP plant have to compare the benefits in power block and receiver with the additional risks and cost. Hering et al. (2012) proposed a sodium thermocline TES working within the temperature span of 200 °C and 550 °C on the intermediate level of a combined cycle CSP plant (see also Section 3.3.1).

## 9.4. Haloglass™ RX

*Haloglass™ RX* is a glass consisting of stable and low-cost components. The upper thermal limit is given by the manufacturer, Halotechnics (2013), as 1200 °C, which would qualify it as the sensible heat TES medium of the investigated future Rankine or Brayton cycles. However, at 450 °C the lower operating limit is high as well and creates freeze protection challenges. This limit is not dictated by thermal stability or phase change, but by its very high viscosity, which is a typical phenomenon of glasses. The manufacturer states that at this temperature, the viscosity reaches a pumpability limit of 10 000 mPa s. It is expected that even though technically feasible, operating at these conditions will not be desirable, so that the upper operating temperature will be considerably higher. At high viscosities, turbulent flow is difficult to reach and, therefore, convective heat transfer is limited.

The thermal conductivity of *Haloglass™ RX* is mediocre at an estimated value of 0.8 W/m K. The influence of radiative heat transfer inside the liquid is assumed to be low because of its low transmissivity in the emission spectrum up to 1000 °C (Shand, 1958). However, this has to be investigated further. More information on this topic can be found in works by Shand, Turkdogan (1983) and Mann et al. (1992).

The volumetric heat capacity, that is the product of density and specific heat capacity, of *Haloglass™ RX* is approximately 20 % higher than that of *Solar Salt™*. Glasses can have widely varying costs and the price and availability of *Haloglass™ RX* could not be identified at this stage. However, due to its proposed application as a "grid scale thermal electricity storage system", it is assumed to be cost competitive to other TESS solutions.

## 9.5. Steam/Water

Steam separators are normal components in (subcritical) steam power cycles. They provide a simple means of separating saturated steam from saturated water in an evaporation process in order to ensure the steam quality downstream of the evaporator (in the inlet of the superheater or steam turbine). The mass inside the steam drum already adds some thermal inertia to the system, however, in CSP plant employing DSG, additional inertia is needed for longer cloudy periods or to enable dispatchability of power generation.

*Abengoa Solar's Planta Solar 10* (*PS10*) power plant uses four pressurized tanks as so called "steam accumulators". These store excess thermal energy in times of high irradiation in the form of saturated water, which can be released as steam of continuously decreasing pressure (sliding pressure) when needed. This means that the tanks have to store water at live steam pressure (40 bar in the case of *PS10*), which makes big volumes

unviable. At a capacity of 20 MW $h_t$, the vessels of the plant only deliver enough energy to run the turbine at 50 % of the nominal load for 50 minutes (see Solúcar, 2006). *Abengoa Solar's* second commercial solar power tower plant *PS20* has the same storage properties while the nominal power rating of the plant is 20 $MW_e$. The TESS is, therefore, only a buffer which means that its purpose is to overcome short-term transients. According to Laing et al. (2011), there is no other storage technology commercially available for DSG plants than steam accumulators and these are not cost-competitve for long-term storage.

Steinmann and Eck (2006) investigated different configurations of steam accumulators as TESS. One of them uses a sensible passive concrete heat store in series to the accumulator for superheating the saturated steam (Figure 11(a)). Another one (Figure 11(b)) features a PCM as filler material in order to enhance the volumetric heat capacity.

Bai and Xu (2011) also investigated a cascaded TESS for DSG plants, consisting of a steam accumulator and a sensible heat concrete storage. They modeled the thermal behavior of both TES units during discharging and found a big influence of the thermal conductivity of the sensible storage on the discharging performance.

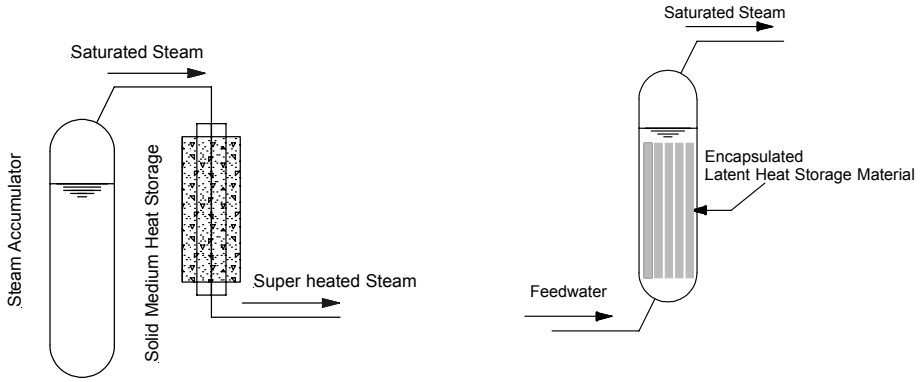


Figure 11: Enhanced steam accumulators: (a) superheater in series, (b) latent heat filler material (Steinmann and Eck, 2006)

## 10. Media for Passive Sensible TESS/Filler Material

Solid filler materials are proposed to enhance the thermocline in single-tank TESSs and substitute expensive/low-thermal-capacity fluid with solids of higher specific thermal capacity, higher density and/or lower cost. Popular concepts are packed beds of spheres or natural rocks and high-temperature concrete blocks.

### 10.1. Packed Beds

Li et al. (2011) and Flueckiger et al. (2013) gave elaborate overviews on heat transfer in packed beds and its modeling.

An unsolved problem of packed bed TESS is an effect called 'ratcheting'. The term describes mechanical stresses on the bed material and on the containment during charging/discharging due to their differing thermal expansion factors (see Figure 12). Dreißigacker et al. (2010), Dreißigacker and Zunft (2012) and Dreißigacker et al. (2013) described the thermo-mechanical modeling and testing of packed bed TESSs. The investigated system was a tank filled with spherical ceramic particles, which was charged and discharged with unpressurized air of 550 °C and 20 °C, respectively. They found the mechanical stresses on the containment to be "moderate and manageable".

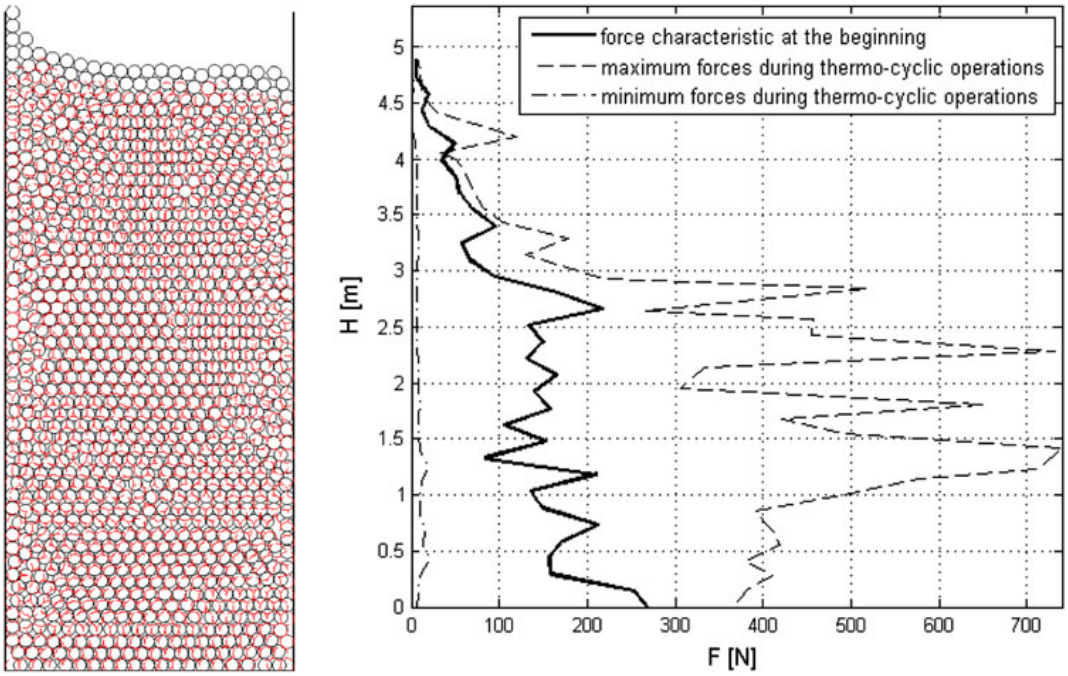


Figure 12: Rearrangement of particles after several cycles (left) and radial average forces before and during cycling (Dreißigacker and Zunft, 2012).

Spelling et al. (2012) conducted techno-economic analyses of hybridized solar gas turbine plants with and without storage. The TESS was situated downstream of the pressurized receiver and, therefore, pressurized itself. They proposed an insulated steel vessel filled with a packed bed of magnesia fire bricks.

## 10.2. Rocks and Sand

A packed bed storage built of locally abundant rocks that are virtually cost-free enables very cost effective designs. Such storages also have excellent environmental and safety properties: They cannot explode, catch fire (except for insulation material perhaps) or leak toxic substances and almost no $CO_2$ is released during manufacturing.

Pacheco et al. (2002) investigated and tested a small pilot-scale thermocline TES with molten salt as the transport medium and different rock and sand filler materials.

They concluded that a combination of **quartzite rock and silica sand** would be most appropriate for costs and low voidage fraction because of the different particle sizes. This concept has been used in the *Solar One* plant before. Brosseau et al. (2005) reported on several long-term isothermal (1 year) and thermally cycled (10 000 cycles) tests of these filler materials in molten salt environments at temperatures of up to 500 °C. The filler materials themselves did not show any sign of deterioration, however, at least at the highest temperatures, the *HITEC® XL* molten salt did cause extensive corrosion and deterioration.

Yang and Garimella (2010) simulated the temperature distribution during charging and discharging in a **quartzite rock** bed TES with molten salt as the HTF. They found a strong dependence of the tank insulation and Reynolds number on the outlet temperature. Xu et al. (2012) modeled the development of a similar thermocline during standby.

Schneider et al. (2011) announced the commercialization of a modular packed bed storage TESS made of **rock or sand**. They use ambient air as the secondary HTF of the storage system with a heat exchanger separating it from the receiver cycle, which could be omitted if air is the primary HTF as well.

Hänchen et al. (2011) developed and validated a thermal model of an air-charged packed bed TESS. They investigated the influence of different storage materials (rocks, aluminium, steel, steatite), tank height, mass flow rate and particle diameter.

Zavattoni et al. (2011) and Zanganeh et al. (2012) investigated, modeled and conducted experiments on a 6.5 MW $h_t$ pilot-scale conical packed bed of rocks, which was charged with ambient air at temperatures up to 500 °C and contained by a concrete structure (see Figure 13). Zavattoni et al. conducted CFD simulations to find pressure drops and temperature distribution and compared it to experimental results with **steatite rocks** with an average diameter of 3 cm as the storage medium. The properties of this and other types of storage media that were considered, can be found in APPENDIX B.1. It can be seen, that thermal conductivity of the rocks changes considerably within the measuring range of 25 °C to 175 °C.

Allen (2010) and Allen et al. (2012) experimentally investigated pressure drop, heat transfer and thermal cycling stability of packed beds of rock. Of the several different types of locally (Northern Cape, South Africa) available rock samples, two, namely **dolerite and granite**, did not show failures when thermally cycled between ambient temperature and 510 °C. They found a strong dependency of the pressure drop - and therefore the heat transfer - on the packing direction of the rocks. Randomly poured beds will, thus, have a high uncertainty in performance. However, the thermal performance appeared favorable and, based on these experiments, Heller and Gauché (2013) investigated the performance of a rock bed TESS in a combined cycle CSP plant.

Schwaiger et al. (2012) and Haider et al. (2012) investigated and modeled a cascaded sensible/latent TESS for DSG CSP plants. The sensible storage medium of the superheating section is **sand**, which is being transported through the heat exchangers via fluidization in air. The aspired maximum storage temperature is approximately 600 °C. No details on the properties of the used sand could be retrieved.

Future CR plants with supercritical HTFs (s-$H_20$ and s-$CO_2$) proposed by Kelly (2010)

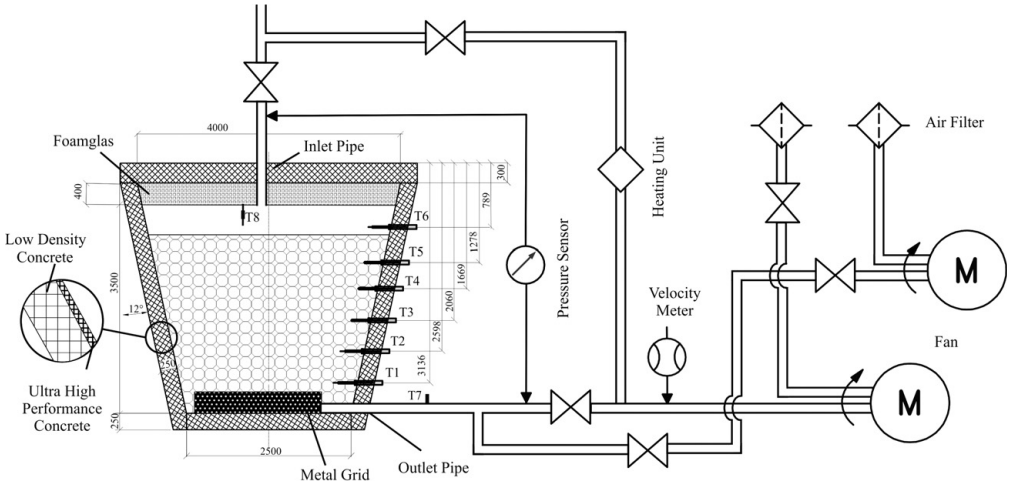


Figure 13: Scheme of the conical rock bed system as set-up by Zanganeh et al. (2012).

feature packed bed thermoclines as the TES. The vessels containing these beds of **ceramics or quartzite rocks** have to withstand the very high pressures of the HTF. According to Kelly, "The most economical pressure vessel is a commercial section of standard pipe [...]". When the largest standard pipes with the necessary wall thickness are used, thousands of these are needed to enable dispatchability of the plant. The maximum operating temperature of the TESS is supposed to be approximately 650 °C, the particle diameter 5 mm. Capital cost estimates show, that the TESS of the proposed supercritical plants are about ten times more expensive than molten salt tank systems. This is mainly due to the considerably larger amount of high-temperature steel needed. Even much higher efficiencies in supercritical plants cannot compensate for this handicap.

## 10.3. Concrete

Tamme et al. (2003) and Laing et al. (2006) proposed and tested a sensible passive TESS employing blocks of concrete and castable ceramic, embedding pipes that the HTF passes through. The project mainly aimed at the development of a low cost storage due to a cheap storage medium for DSG parabolic trough plants. Concrete was found to be the more fitting material of the two in terms of cost and durability. Improved tube arrangements, distances and enhancements (for example, fins) have been investigated (Laing et al., 2008; Laing, Bahl, Bauer, Fiss, Breidenbach and Hempel, 2012) and, as an advancement, Laing et al. (2010) investigated a serial arrangement of sensible concrete TESSs for pre- and superheating of steam and a PCM storage for evaporation. The concept has been tested with a rating of 1 MW $h_t$ as part of a DSG test facility at a conventional power plant (Laing et al., 2011; Laing, Eck, Hempel, Johnson, Steinmann, Meyer and Eickhoff, 2012). The used concrete is thermally stable up to 500 °C after

several initial heating cycles, in which mass and tensile strength decrease considerably. Further material details of high-temperature concrete and castable ceramics can be found in APPENDIX B.1.

Brown et al. (2012) and Selvam and Strasser (2012) proposed bricks and parallel plates of concrete in a vessel that are in direct contact to the HTF as the filler material of a TESS. The main advantage of this concept as compared to packed beds is that ratcheting is avoided. The concrete withstood thermal cycling between 300 °C and 600 °C. Thermal conductivity was given with 2 W/m K, specific heat capacity with 900 J/kg K and the storage material costs were estimated at 0.78 to 3.18 USD/kW $h_t$.

## 10.4. Ceramics

Glück et al. (1991) tested a composite sensible/latent TES consisting of ceramic bricks with molten salt as the PCM. According to Glück et al., the concept can be explained as "microencapsulation of a PCM within the submicron pores of a ceramic matrix." Experiments were run with air of up to 1300 °C as the HTF.

As mentioned in Section 10.3, Laing et al. (2006) tested castable ceramic as the storage medium for parabolic trough DSG plants but found high-temperature concrete more appropriate for its low price and good thermal stability, despite its lower specific storage capacity and thermal conductivity.

Dreißigacker et al. (2013) modeled a packed bed built of ceramic spheres for application as a TESS for CSP. The focus of their work was on the thermally induced stresses on the walls and spheres and they didn't state the type of ceramic they used, but gave some properties that can be found in B.1.

Zunft, Hänel, Krüger, Dreißigacker, Göhring and Wahl (2011) reported on gained experience from the passive TES subsystem of the *Jülich Solar Power Tower*. "Its TES design is based on refractory bricks in honeycomb shape in a stacked arrangement." (Dreißigacker and Zunft, 2012). The storage is being charged and discharged with unpressurized air at 680 °C and 150 °C, respectively. The discharge heat rate reached 5.7 $MW_t$ at an "almost constant" temperature of 640 °C for approximately 1.5 hours. The principle thermal and mechanical performance of the system was confirmed, the pressure drop was lower than expected. In another study, Zunft, Hahn and Kammel (2011) modeled the air flow distribution "[...] in an isotropic porous medium, a well founded assumption in particular in the case of ceramic honeycombs or packed beds with large specific heat transfer surfaces." They found that the inlet and outlet air distribution system had a considerable influence on flow distribution and, therefore, useful thermal capacity of the TESS.

## 10.5. Graphite

Forsberg et al. (2007) proposed graphite as the filler material in the TES of a plant with high-temperature fluoride salt as the HTF. Graphite is chosen for its compatibility with molten salts at high temperatures, its low cost, high heat capacity and thermal conductivity (see APPENDIX B.1). According to the authors, graphite has been used

in contact with fluoride salts at temperatures of approximately 1000 °C in the aluminium industry for decades and the cost of these high performance graphites is less than *SunShot* cost goals.

## 11. Latent Heat Storage Media

The determining property of 'classical' (eutectic) latent heat TESS (LHTESS) is that heat is added and rejected at a constant temperature (normally the melting temperature). This ensures constant operating conditions of heat exchangers and turbomachinery. However, the discharge rate might be non-constant because of differing heat transfer effects due to solidification of the phase change material (PCM) around heat exchanger tubes (see Figure 14). The other aspired advantage of a TESS employing PCMs, besides the constant temperature, is the high energy density and therefore smaller mass of the storage medium and volume of the tank.

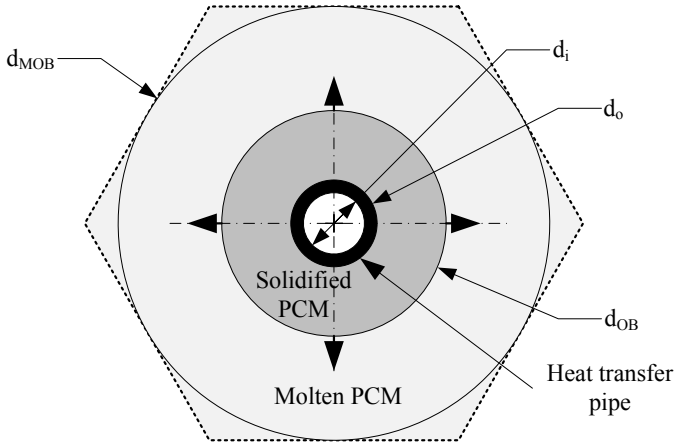


Figure 14: Scheme of the cross-section of a heat transfer pipe in a latent heat TES (Kotzé, Backström and Erens, 2012*b*).

Hoshi et al. (2005) did a screening of potential PCMs for linear Fresnel and CR applications. The most important property is obviously the temperature at which the phase change happens. Because of the specific volume and required pressure, this is almost exclusively the melting temperature and not the evaporation temperature. In the region of melting temperatures $> 500\,°C$, which is relevant for high-efficiency cycles, all PCMs investigated by Hoshi et al. are salts. Figure 15 shows the respective melting points of these salts at ambient pressure and another very important property for system cost reduction: the volumetric heat capacity. The third important thermophysical property of PCMs is thermal conductivity. Low values of it create high thermal resistances during charging and discharging and, therefore, limit the possible heat flux of the TESS or require additional heat transfer surfaces (for example, a greater number of pipes or finned pipes). Besides the qualities given above, Liu et al. (2012) also named the following as

important aspects of storage media: chemically stabile, non-corrosive, non-hazardous, congruent melting, insignificant supercooling and low cost.

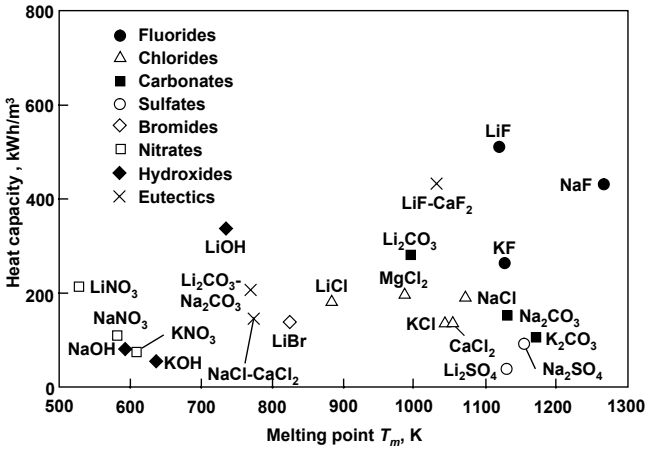


Figure 15: Volumetric heat capacity and melting point of investigated salt PCMs (Hoshi et al., 2005).

Conductivity enhancing methods for LHTESS have been investigated and reviewed by Fan and Khodadadi (2011), Agyenim et al. (2010), Liu et al. (2012) and Robak et al. (2011), who proposed heat pipes connected to the HTF pipes. Liu et al., Zalba et al. (2003), Gil et al. (2010) and Kenisarin (2010) also reviewed PCMs in the temperature range (see APPENDIX B.2).

## 11.1. Salts

Laing et al. (2010) describe a combined sensible/latent heat TESS with concrete and **$NaNO_3$** as the storage media. The enthalpy of fusion of $NaNO_3$ is 175 kJ/kg at a melting temperature of 306 °C. This temperature is appropriate for a superheated DSG plant with charging and discharging pressures of 107 bar and 81 bar, respectively. Detailed thermophysical properties of $NaNO_3$ and its melting behavior can be found in Bauer et al. (2009) and APPENDIX B.2. Test results for a pilot combined TESS, which has been installed at a conventional power plant, show that the used finned tubes in the 700 kW $h_t$ LHTESS improved the discharging rate significantly (Laing, Eck, Hempel, Johnson, Steinmann, Meyer and Eickhoff, 2012). Schwaiger et al. (2012) used the same storage medium for the latent heat part of their modeled TESS, however, with sand as the storage medium to provide the sensible heat needed for superheating steam (see Section B.2).

Zipf et al. (2012) developed and tested a screw heat exchanger for the phase change process in a latent heat TESS based on **Solar Salt**™ as the PCM. The heat exchanger is intended for a DSG cycle at an evaporation temperature of 221 °C. According to the authors, this technology could also be used for other molten salts, for instance, $NaNO_3$, to reach higher evaporation temperatures, pressures and efficiency.

## 11.2. Metals

Blanco-Rodríguez et al. (2012) screened different metal compositions for the use as PCMs in DSG plants. They decided on the eutectic magnesium-zinc alloy with 49 % by mass of magnesium (**MgZn51**) as the most suitable one and conducted thermo-chemical experiences. During 20 freeze-melt cycles, they confirmed literature values between 340 °C and 343 °C for the melting temperature and measured the enthalpy of fusion, however, they did not state the result for it.

Kotzé, Backström and Erens (2012*a*) investigated the eutectic aluminium-silicon alloy with 12 % by mass of silicon, **AlSi12**, as the storage medium in between the superheated steam power cycle and a molten metal cycle on the receiver side. The chosen molten metal of eutectic sodium and potassium (NaK78) reacts highly exothermic with water, so that the chosen TESS also acts as a separating heat exchanger between the two cycles (see Figure 16). The enthalpy of fusion of the eutectic composition is given with 549 kJ/kg at a melting temperature of 577 °C, which agrees well with state of the art superheated steam cycles' requirements but is low for high efficiency supercritical steam cycles. A possible next generation TESS is proposed to use different metal alloys instead, for example, **MgSi56**, at a melting temperature of 946 °C.

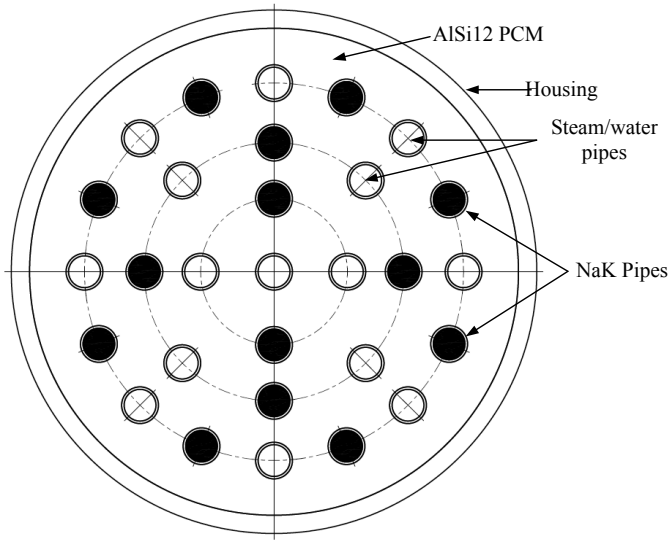


Figure 16: AlSi12 heat exchanger/TESS (Kotzé, von Backström and Ehrens, 2012).

Non-eutectic PCMs do not have a distinct melting temperature but rather a temperature range in which the composition liquifies/solidifies (liquidus to solidus temperature). In order to store energy at a higher temperature and especially if heat is not needed at a constant temperature but over a temperature range, for instance, for superheating or supercritical heating, non-eutectic compositions can be preferable storage media.

Hunt and Carrington (2012) proposed hypereutectic compositions of aluminium-silicon alloys, that is compositions with a higher mass percentage of silicon than 12.6 % (see

Figure 17), as the PCM. The liquidus temperature of **hypereutectic Al-Si** compositions rises up to a maximum of 1414 °C for pure silicon, which enables energy storage at temperature levels at the inlet of state of the art gas turbines expanders.

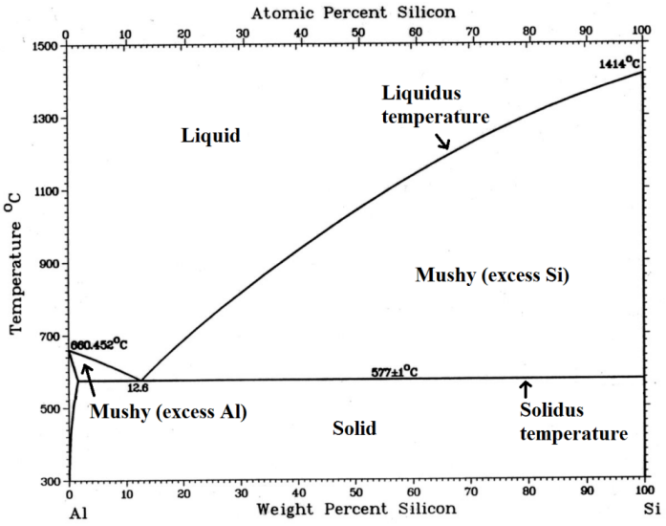


Figure 17: Equilibrium phase change diagram for Al-Si alloys (Hunt and Carrington, 2012).

Because of the combined temperature rise and phase change, the effective specific heat capacity changes during non-eutectic phase change depending on initial composition (see Figure 18). Heat transfer of hypereutectic Al-Si alloys is good at thermal conductivities between 190 W/m K for pure silicon and 60 W/m K for AlSi12. The density of Al-Si alloys is relatively high and the density change during melting is small, so that no rupturing is to be expected, but measurable, which could support natural convention within heat exchanger tanks. According to Hunt and Carrington (2012), Al-Si alloys are also non-degrading, affordable, available and well known to the industry. The PCM has to be contained in a material that is able to withstand the high temperatures and (possibly) pressures and doesn't cause any corrosion issues.

## 12. Chemical Potential Storage Media

Chemical potential TESS store heat by supplying it to reversible endothermic chemical reactions. According to Tian and Zhao (2013), the three most important properties of the reaction in such a system are: chemical reversibility, large enthalpy change and simple reaction conditions. Because of the very high energy densities of the reaction products, the technology even enables the production of solar fuels, which is being researched extensively by the Professorship of Renewable Energy Carriers (2013) at the Swiss Federal Technical University (ETH) Zurich. However, the technology is still in an experimental to pre-commercial stage, therefore, it is not being reviewed in detail.

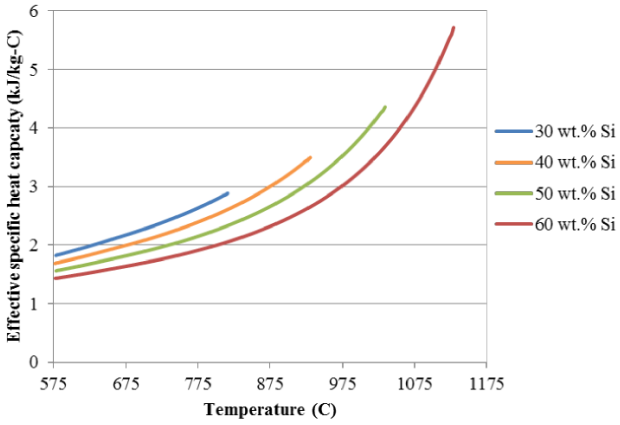


Figure 18: Changing effective specific heat capacities of Al-Si alloys during melting (Hunt and Carrington, 2012).

## 13. System Considerations

The example of LHTESSs demonstrates the importance of fitting a storage system to the characteristics of the power block and receiver system. The advantages of PCMs are obvious (high specific capacity and constant stable temperatures). The latter can be implemented favorably into a saturated/superheated steam power cycle, in which large amounts of heat are required at a constant temperature for evaporation of the working fluid. This is even more true if the HTF undergoes a phase change as well, as, for example, in DSG plants (see Figure 19). However, using a TESS consisting of only one PCM and no sensible storage, would result in high exergetic losses and unnecessary high receiver inlet temperatures. In most studies, LHTESS have been proposed as one part of the storage system for DSG plants (see, for example, Birnbaum et al., 2008; Laing et al., 2010; Feldhoff et al., 2012; Schwaiger et al., 2012). Usually, energy for superheating and possibly preheating of the working fluid are supplied by sensible heat TESS and only its heat of evaporation is delivered at constant temperature by the PCM (see Figure 19).

Michels and Pitz-Paal (2007) proposed a cascaded TESS of several PCMs in series for parabolic trough power plants using state of the art oil as the HTF. The temperature range of the TESS was therefore approximately 300 °C to 400 °C. The chosen PCMs with their respective melting temperatures and heats of fusion can be found in Figure 20.

An additional application of a (small) LHTESS is the stabilization of the steam generator inlet temperature. In such a system, the PCM would buffer transients through its high enthalpy of fusion.

Birnbaum et al. (2008) compared two different options of implementing the storage system in a DSG plant. In both, the TESS is charged with live steam at nominal 110 bar and discharged at 75 bar, which is due to the temperature gradient in the TESS during charging and discharging. However, when the solar field only generates enough energy to run the power cycle in part load (see Figure 21), the two options differ: In the first

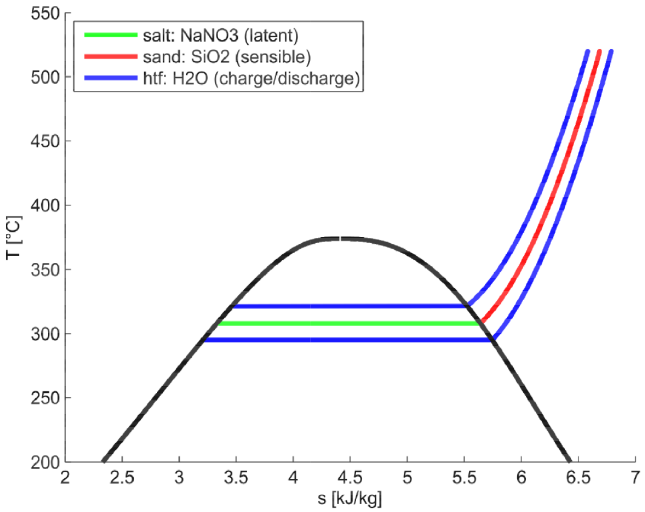


Figure 19: T-s diagram depicting charging and discharging of a cascaded latent and sensible heat TESS (Schwaiger et al., 2012).

one, additional steam mass flow will be added once the live steam pressure reaches the discharging pressure of the TESS (75 bar), in the second one, steam generated in the TESS only enter the steam turbine after the initial blade rows when the steam from the solar field is expanded to the pressure level of storage discharge.

Aga et al. (2012) proposed a DSG plant layout in which the turbine-generator system produces as much energy during storage discharging mode as in 'solar' mode. This is achieved by shutting down the high pressure stage and feeding the intermediate and low pressure stages of the turbine with higher pressure steam than during nominal load.

Zaversky et al. (2012) compared single-train to parallel dual-train oil-to-salt heat exchanger configurations for parabolic trough plants. They conclude that the performance of the parallel concept is much more favorable in part-load because one train could be completely shut off instead of strongly decreasing the oil mass flow and, therefore, the heat transfer coefficient.

Yogev and Kribus (2012) investigated the discharging behavior of the LHTES part of the latent/sensible hybrid TESS in a CSP plant. They build a simple model of a LHTES with $NaNO_3$ as the PCM and compared different discharging modes with different heat flux reduction rates. They found that the power cycle's electricity output can be controlled to be nearly constant when it is run in sliding pressure mode and the flow rate is increased accordingly during discharging.

## 14. Modeling of TESS

Powell and Edgar (2012) described the basic modeling of a CSP plant consisting of collector, TESS, boiler and control system. Li et al. (2011) states analytical equations

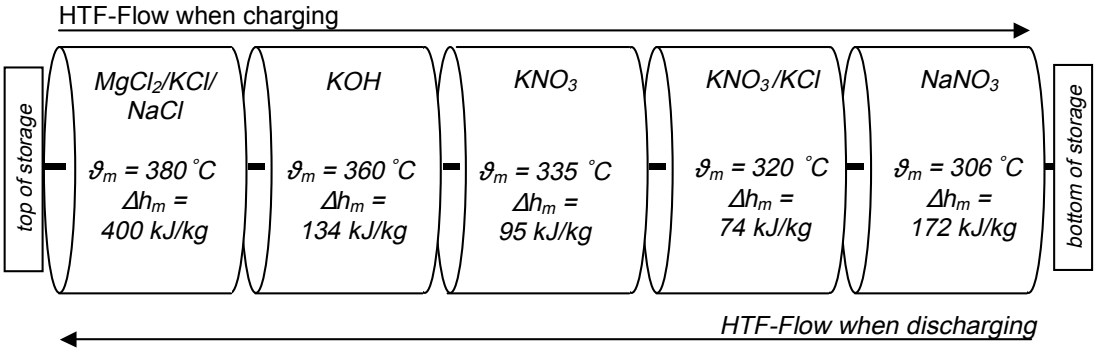


Figure 20: Sketch of a cascaded LHTESS including melting temperatures and heats of fusion (Michels and Pitz-Paal, 2007).

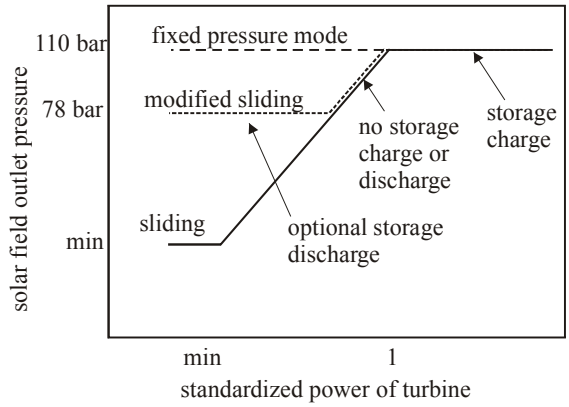


Figure 21: Pressure characteristics of DSG cycle at part-load (Birnbaum et al., 2008).

and numerical approaches for modeling of packed bed passive TESS and LHTESSs. Van Lew et al. (2011) compared simulations with the model for packed beds by Li et al. with eperimental results from the literature. The thermo-mechanical modeling of a packed bed TES was demonstrated by Dreißigacker et al. (2010). Zanganeh et al. (2012) modeled a rock bed TESS and validated the model by low-temperature experiments on a 6.5 MW $h_t$ demonstration system. Flueckiger et al. (2011*b*) built a thermo-mechanical model of a TESS that consists of solid filler material (rock and sand) and oil as the active medium in the storage loop. The validation with data from the *Solar One* demonstration plant shows good agreement in predicting thermal ratcheting. In (Flueckiger et al., 2011*a*), the active medium was changed to molten salt (*HITEC® Heat Transfer Salt*) and the filler material was only quartzite rock. Xu et al. (2012) modeled a molten salt thermocline tank, varied inlet velocity, porosity, inlet temperature and tank height and showed the influence on the thermocline quality after various time steps of standby. Yogev and Kribus (2012) modeled an DSG plant including an LHTESS. They simulated

the charging and discharging behavior for different thermal conductivity values in sliding pressure mode.

## References


Aga, V., Ehrsam, A., Boschek, E., Breschi, D. and Girard, R. (2012), Thermal Energy Storage And Turbine Solution For Direct Steam Solar Power Plants With Nominal Power Output During Storage Discharge, *in* 'SolarPACES 2012', Marrakech, Morocco.

Agyenim, F., Hewitt, N., Eames, P. and Smyth, M. (2010), 'A review of materials, heat transfer and phase change problem formulation for latent heat thermal energy storage systems (LHTESS)', *Renewable and Sustainable Energy Reviews* **14**(2), 615–628.
**URL:** *http://linkinghub.elsevier.com/retrieve/pii/S1364032109002469*

Allen, K., Backström, T. V. and Kröger, D. (2012), Packed Beds of Rock for Thermal Storage, *in* '1st Southern African Solar Energy Conference', Stellenbosch, South Africa, pp. 1–9.

Allen, K. G. (2010), Performance characteristics of packed bed thermal energy storage for solar thermal power plants, M.sc. eng, University of Stellenbosch.
**URL:** *http://hdl.handle.net/10019.1/4329*

An, D. (2011), Sodium fire suppression using liquid nitrogen, M.sc., University of Maryland.
**URL:** *http://drum.lib.umd.edu/bitstream/1903/12385/1/An_umd_0117N_12846.pdf*

Aora Solar Ltd (2012), 'AORA'.
**URL:** *http://aora-solar.com/*

Ávila Marín, A. L. (2011), 'Volumetric receivers in Solar Thermal Power Plants with Central Receiver System technology: A review', *Solar Energy* **85**(5), 891–910.
**URL:** *http://www.sciencedirect.com/science/article/pii/S0038092X11000302*

Bai, F. and Xu, C. (2011), 'Performance analysis of a two-stage thermal energy storage system using concrete and steam accumulator', *Applied Thermal Engineering* **31**(1415), 2764–2771.

Bauer, T., Breidenbach, N., Pfleger, N., Laing, D. and Eck, M. (2012), Overview of Molten Salt Storage Systems and Material Development for Solar Thermal Power Plants, Technical report, DLR.
**URL:** *https://ases.conference-services.net/resources/252/2859/pdf/SOLAR2012_0122_fullpaper.pdf*

Bauer, T., Laing, D., Kröner, U. and Tamme, R. (2009), Sodium Nitrate for High Temperature Latent Heat Storage, *in* '11th International Conference on Thermal Energy Storage', Stockholm, Sweden.
**URL:** *http://talon.stockton.edu/eyos/energy_studies/content/docs/effstock09/Session_3_1_Efficient_Soultions_using_short_term_TES/4.pdf*

Becker, M. (1980), 'Comparison of heat transfer fluids for use in solar thermal power stations', *Electric Power Systems Research* **3**(3-4), 139–150.
**URL:** *http://linkinghub.elsevier.com/retrieve/pii/0378779680900012*

Birnbaum, J., Eck, M., Fichtner, M., Hirsch, T., Pitz-Paal, R. and Zimmermann, G. (2008), A Concept for Future Parabolic Trough Based Solar Thermal Power Plants, *in* 'ICPWS', Berlin.
**URL:** *www.15icpws.de/papers/10_Green-02_Birnbaum.pdf*

Blanco-Rodríguez, P., Rodríguez-Aseguinolaza, J., Faik, A., Calvet, N., Tello, M. J. and Doppiu, S. (2012), Eutectic Metal Alloys as Phase Change Material for Thermal Energy Storage in Concentrated Solar Power, *in* 'SolarPACES 2012', Marrakech, Morocco.

Boerema, N., Fisher, J., Morrison, G. and Rosengarten, G. (2011), A Comparison of High Temperature Heat Transfer Fluids for Concentrating Solar Thermal Systems, *in* 'SolarPACES 2011', Vol. 2, Granada, Spain.

Boerema, N., Morrison, G., Taylor, R. and Rosengarten, G. (2012), 'Liquid sodium versus Hitec as a heat transfer fluid in solar thermal central receiver systems', *Solar Energy* **86**(9), 2293–2305.
**URL:** *http://www.sciencedirect.com/science/article/pii/S0038092X12001703*

Boss, M., Gadoury, T., Feeny, S. and Montgomery, M. (2007), Recent Advances in Ultra Super Critical Steam Turbine Technology, Technical report.
**URL:** *http://www.ge-energy.com/content/multimedia/_files/downloads/article-GE1000MWUSCpaperwithedits2-1-10.pdf*

Brosseau, D., Kelton, J. W., Ray, D., Edgar, M., Chisman, K. and Emms, B. (2005), 'Testing of thermocline filler materials and molten-salt heat transfer fluids for Thermal energy storage systems in parabolic trough power plants', *Journal of solar energy engineering* **127**(1), 109–116.
**URL:** *http://cat.inist.fr/?aModele=afficheN&cpsidt=16586587*

Brown, B. M., Strasser, M. N. and Selvam, R. P. (2012), Development of a Structured Thermocline Thermal Energy Storage System, pp. 1–8.
**URL:** *http://ases.conference-services.net/resources/252/2859/pdf/SOLAR2012_0074_fullpaper.pdf*

Cabeza, L. F., Sole, C., Castell, A., Oro, E. and Gil, A. (2012), Review of Solar Thermal Storage Techniques and Associated Heat Transfer Technologies, *in* 'Proceedings of the IEEE', Vol. 100, pp. 525–538.
**URL:** *http://ieeexplore.ieee.org/xpls/abs_all.jsp?arnumber=5942138&tag=1*

Cengel, Y. and Boles, M. (2010), *Thermodynamics: An Engineering Approach with Student Resources DVD*, McGraw-Hill Science/Engineering/Math.

Chapman, D. J. and Arias, D. A. (2009), An Assessment of the Supercritical Carbon Dioxide Cycle for Use in a Solar Parabolic Trough Power Plant, *in* 'Proceedings of SCCO2 Power Cycle Symposium 2009', Troy, NY.

Chen, H., Chen, Y., Hsieh, H.-T. and Siegel, N. (2007), 'Computational Fluid Dynamics Modeling of Gas-Particle Flow Within a Solid-Particle Solar Receiver', *Journal of Solar Energy Engineering* **129**(2), 160.
**URL:** *http://link.aip.org/link/JSEEDO/v129/i2/p160/s1&Agg=doi*

Coastal Chemical Co. (n.d.*a*), 'HITEC Heat Transfer Salt'.
**URL:** *http://www.coal2nuclear.com/MSR-HITECHeatTransferSalt.pdf*

Coastal Chemical Co. (n.d.*b*), 'Hitec Solar Salt'.

Cordaro, J. G., Kruizenga, A. M., Altmaier, R., Sampson, M. and Nissen, A. (2011), Thermodynamic properties of molten nitrate salts, *in* 'SolarPACES 2011', Vol. 1, Sandia National Laboratories, Seville, Spain.
**URL:** *http://energy.sandia.gov/wp/wp-content/gallery/uploads/Thermodynamic-Porperties-of-Molten-Nitrate-Salts-Cordaro.pdf*

Coventry, J. and Pye, J. (2010), Coupling Supercritical and Superheated Direct Steam Generation with Thermal Energy Storage, Technical report, Wizard Power.
**URL:** *http://solar-thermal.anu.edu.au/files/2010/02/SolarPACES2009_CoventryPye.pdf*

Cox, T. L. (2009), Preliminary Results of Heat Transfer Experiments with Supercritical Carbon Dioxide in the Small System Test Loop, *in* 'Proceedings of SCCO2 Power Cycle Symposium 2009', Troy, NY.

Crocker, A. and Miller, F. (2011), Fluid Flow and Radiation Modeling of a Cylindrical Small Particle Solar Receiver, *in* 'SolarPACES 2011', Granada, Spain.

Diver, R. B., Adkins, D. R. and Moss, T. A. (1990), Trends in Dish-Stirling Solar Receiver Designs, *in* 'Energy Conversion Engineering Conference', pp. 303–310.
**URL:** *http://ieeexplore.ieee.org/xpls/abs_all.jsp?arnumber=747967*

DLR (2010), Solar-Hybrid Power and Cogeneration Plants, Technical Report 019830, Deutsches Zentrum für Luft- und Raumfahrt e.V.
**URL:** *http://www.fzea.usp.br/green/solhyco/upload/Solhyco_final_report.pdf*

Dostal, V., Driscoll, M. J. and Hejzlar, P. (2004), A Supercritical Carbon Dioxide Cycle for Next Generation Nuclear Reactors, Technical report, Massachusetts Institute of Technology, Cambridge, MA.

Dow Chemical Company (2001), 'Synthetic Organic Heat Transfer Fluid Liquid and Vapor Phase Data'.
**URL:** *http://www.dow.com/webapps/lit/litorder.asp?filepath=heattrans/pdfs/noreg/176-01463.pdf&pdf=true*

Dreißigacker, V., Müller-Steinhagen, H. and Zunft, S. (2010), 'Thermo-mechanical analysis of packed beds for large-scale storage of high temperature heat', *Heat and Mass Transfer* **46**(10), 1199–1207.
**URL:** *http://www.springerlink.com/index/10.1007/s00231-010-0684-5*

Dreißigacker, V. and Zunft, S. (2012), Thermo-mechanical implications of packed bed heat storage for CSP : A Modeling approach and a simulation study for a large- scale application, *in* 'SolarPACES 2012', Marrakech, Morocco.

Dreißigacker, V., Zunft, S. and Müller-Steinhagen, H. (2013), 'A thermo-mechanical model of packed-bed storage and experimental validation', *Applied Energy* .
**URL:** *http://linkinghub.elsevier.com/retrieve/pii/S0306261913002638*

Duffie, J. A. and Beckman, W. A. (1991), *Solar Engineering of Thermal Processes*, 2nd edn, John Wiley & Sons, Inc., New York.

Dunn, R. I., Hearps, P. J. and Wright, M. N. (2012), Molten-Salt Power Towers: Newly Commercial Concentrating Solar Storage, *in* 'Proceedings of the IEEE', Vol. 100, pp. 504–515.

EC (2005), Solar hybrid gas turbine electric power system, Technical report, European Commission, Brussels.
**URL:** *http://bookshop.europa.eu/en/solgate-solar-hybrid-gas-turbine-electric-power-system-pbKINA21615/downloads/KI-NA-21-615-EN-C/KINA21615ENC_002.pdf?FileName=KINA21615ENC_002.pdf&SKU=KINA21615ENC_PDF&CatalogueNumber=KI-NA-21-615-EN-C*

Eck, M. and Zarza, E. (2006), 'Saturated steam process with direct steam generating parabolic troughs', *Solar Energy* **80**(11), 1424–1433.
**URL:** *http://www.sciencedirect.com/science/article/pii/S0038092X06000892*

Fan, L. and Khodadadi, J. (2011), 'Thermal conductivity enhancement of phase change materials for thermal energy storage: A review', *Renewable and Sustainable Energy Reviews* **15**(1), 24–46.
**URL:** *http://linkinghub.elsevier.com/retrieve/pii/S1364032110002595*

Feldhoff, J. F., Schmitz, K., Eck, M., Schnatbaum-Laumann, L., Laing, D., Ortiz-Vives, F. and Schulte-Fischedick, J. (2012), 'Comparative system analysis of direct steam generation and synthetic oil parabolic trough power plants with integrated thermal storage', *Solar Energy* **86**(1), 520–530.
**URL:** *http://www.sciencedirect.com/science/article/pii/S0038092X11003938*

Flueckiger, S. M., Yang, Z. and Garimella, S. V. (2013), 'Review of Molten-Salt Thermocline Tank Modeling for Solar Thermal Energy Storage', *Heat Transfer Engineering* **34**(10), 787–800.
**URL:** *http://dx.doi.org/10.1080/01457632.2012.746152*

Flueckiger, S., Yang, Z. and Garimella, S. V. (2011*a*), 'An integrated thermal and mechanical investigation of molten-salt thermocline energy storage', *Applied Energy* **88**(6), 2098–2105.
**URL:** *http://www.sciencedirect.com/science/article/pii/S0306261910005519*

Flueckiger, S., Yang, Z. and Garimella, S. V. (2011*b*), 'Thermocline Energy Storage in the Solar One Power Plant: An Experimentally Validated Thermomechanical Investigation', *Proceedings of the ASME 2011 5th International Conference on Energy Sustainability* pp. 775–781.
**URL:** *http://dx.doi.org/10.1115/ES2011-54578*

Forsberg, C. W., Peterson, P. F. and Zhao, H. (2007), 'High-Temperature Liquid-Fluoride-Salt Closed-Brayton-Cycle Solar Power Towers', *Journal of Solar Energy Engineering* **129**(2), 141.
**URL:** *http://link.aip.org/link/JSEEDO/v129/i2/p141/s1&Agg=doi*

Foust, O. J. (1972), *Sodium-NaK Engineering Handbook*, Gordon and Breach, Science Publishers, Inc., New York.

Fuller, R. L. and Batton, W. (2009), Practical Considerations in Scaling Supercritical Carbon Dioxide Closed Brayton Cycle Power Systems, *in* 'Proceedings of SCCO2 Power Cycle Symposium 2009', Troy, NY.
**URL:** *http://www.sco2powercyclesymposium.org/resource_center/turbomachinery/practical-considerations-in-scaling-supercritical-carbon-dioxide-closed-brayton-cycle-power-systems*

Furukawa, T., Müller, G., Schumacher, G., Weisenburger, A., Heinzel, A., Zimmermann, F. and Aoto, K. (2004), 'Corrosion Behavior of FBR Candidate Materials in Stagnant Pb-Bi at Elevated Temperature', *Journal of Nuclear Science and Technology* **41**(3), 265–270.
**URL:** *http://www.tandfonline.com/doi/abs/10.1080/18811248.2004.9715484*

Garbrecht, O., Al-sibai, F., Kneer, R. and Wieghardt, K. (2012), Numerical Investigation of a New Molten Salt Central Receiver Design, *in* 'SolarPACES 2012', Marrakech, Morocco.

García, E. and Calvo, R. (2012), One Year Operational Experience of Gemasolar Plant, *in* 'SolarPACES 2012', Marrakech, Morocco.

Gary, J., Turchi, C. and Siegel, N. (2011), CSPand the DOE SunShot Initiative, *in* 'SolarPACES 2011', Vol. 1, Granada, Spain.

Gasanaliev, A. M. and Gamataeva, B. Y. (2000), 'Heat-accumulating properties of melts', *Russian Chemical Reviews* **69**(2), 179–186.
**URL:** *http://stacks.iop.org/0036-021X/69/i=2/a=R07?key=crossref.51b16f738ba53d206a4795cbc793e031*

Gemasolar (2011), 'Gemasolar: how it works'.
**URL:** *http://www.torresolenergy.com/EPORTAL_DOCS/GENERAL/SENERV2/DOC-cw4cb709fe34477/GEMASOLARPLANT.pdf*

Gil, A., Medrano, M., Martorell, I., Lázaro, A., Dolado, P., Zalba, B. and Cabeza, L. F. (2010), 'State of the art on high temperature thermal energy storage for power generation. Part 1 - Concepts, materials and modellization', *Renewable and Sustainable Energy Reviews* **14**(1), 31–55.
**URL:** *http://linkinghub.elsevier.com/retrieve/pii/S1364032109001774*

Glück, A., Tamme, R., Kalfa, H. and Streuber, C. (1991), 'Investigation of high temperature storage materials in a technical scale test facility', *Solar energy materials* **24**(1-4), 240–248.
**URL:** *http://www.sciencedirect.com/science/article/pii/016516339190064R*

Guidez, J., Martin, L., Chetal, S. C., Chellaparndi, P. and Raj, B. (2008), 'Lessons Learned from Sodium-Cooled Fast Reactor Operation and Their Ramifications for Future Reactors with Respect to Enhanced Safety and Reliability', *Nuclear Technology* **164**, 207–220.

Haider, M., Schwaiger, K., Holzleithner, F. and Eisl, R. (2012), 'A Comparison between Passive Regenerative and Active Fluidized Bed Thermal Energy Storage Systems', *Journal of Physics: Conference Series* **395**, 012053.
**URL:** *http://stacks.iop.org/1742-6596/395/i=1/a=012053?key=crossref.e5a818cb0734d0a7d4d832124d7bcd64*

Halotechnics (2012), 'Saltstream 700 Product Overview'.
**URL:** *http://www.halotechnics.com/products/saltstream700.html*

Halotechnics (2013), 'Haloglass RX'.
**URL:** *http://www.halotechnics.com/products/haloglassrx.html*

Hänchen, M., Brückner, S. and Steinfeld, A. (2011), 'High-temperature thermal storage using a packed bed of rocks Heat transfer analysis and experimental validation', *Applied Thermal Engineering* **31**(10), 1798–1806.
**URL:** *http://www.sciencedirect.com/science/article/pii/S1359431111001062*

Heller, L. and Gauché, P. (2013), 'Modeling of the Rock Bed Thermal Energy Storage System of a Combined Cycle Solar Thermal Power Plant in South Africa', *Solar Energy* **93**, 345–356.
**URL:** *http://dx.doi.org/10.1016/j.solener.2013.04.018*

Hennecke, K., Schwarzbözl, P., Hoffschmidt, B., Göttsche, J., Koll, G. and Beuter, M. (2009), The Solar Power Tower Jülich A solar thermal power plant for test and demonstration of air receiver technology, *in* 'Proceedings of ISES World Congress 2007', pp. 1–4.
**URL:** *http://link.springer.com/chapter/10.1007/978-3-540-75997-3_358?LI=true*

Hering, W., Stieglitz, R. and Wetzel, T. (2012), 'Application of liquid metals for solar energy systems', *EPJ Web of Conferences* **33**.
**URL:** *http://dx.doi.org/10.1051/epjconf/20123303003*

Herrmann, U. and Kearney, D. W. (2002), 'Survey of Thermal Energy Storage for Parabolic Trough Power Plants', *Journal of Solar Energy Engineering* **124**(2), 145.
**URL:** *http://link.aip.org/link/JSEEDO/v124/i2/p145/s1&Agg=doi*

Hischier, I., Hess, D., Lipinski, W., Modest, M. and Steinfeld, A. (2009), 'Heat Transfer Analysis of a Novel Pressurized Air Receiver for Concentrated Solar Power via Combined Cycles', *Journal of Thermal Science and Engineering Applications* **1**(4), 041002.
**URL:** *http://link.aip.org/link/JTSEBV/v1/i4/p041002/s1&Agg=doi*

Ho, C. K. (2010), Sandia Advanced Concepts, Technical Report 505, Sandia National Laboratories, Washington D.C.
**URL:** *http://www1.eere.energy.gov/solar/review_meeting/pdfs/prm2010_snl_ho.pdf*

Hoshi, A., Mills, D. R., Bittar, A. and Saitoh, T. S. (2005), 'Screening of high melting point phase change materials (PCM) in solar thermal concentrating technology based on CLFR', *Solar Energy* **79**(3), 332–339.
**URL:** *http://www.sciencedirect.com/science/article/pii/S0038092X04003457*

Hunt, A. J. and Carrington, K. R. (2012), Metal Latent Heat Thermal Storage System, *in* 'SolarPACES 2012', Marrakech, Morocco.

International Atomic Energy Agency (1999), Status of liquid metal cooled fast reactor technology, Technical Report April, International Atomic Energy Agency, Vienna.

Jensch, A., Meschke, F. and Uhlig, R. (2012), 'Pressurized ceramic plate receiver for high outlet temperatures'.

Kadoya, K., Matsunaga, N. and Nagashima, A. (1985), 'Viscosity and thermal conductivity of dry air in the gaseous phase', *Journal of Physical and Chemical Reference Data* **14**(4), 947–970.
**URL:** *http://cat.inist.fr/?aModele=afficheN&cpsidt=8524491*

Kato, Y., Nitawaki, T. and Muto, Y. (2004), 'Medium temperature carbon dioxide gas turbine reactor', *Nuclear Engineering and Design* **230**(1-3), 195–207.
**URL:** *http://linkinghub.elsevier.com/retrieve/pii/S0029549303003935*

Kearney, D. W. (2001), 'Engineering Evaluation of a Molten Salt HTF in a Parabolic Trough Solar Field Concept and Project Overview'.
**URL:** *http://www.nrel.gov/csp/troughnet/pdfs/ulf_herrmann_salt.pdf*

Kelly, B. (2010), Advanced Thermal Storage for Central Receivers with Supercritical Coolants, Technical report, Abengoa Solar, Lakewood, Colorado.
**URL:** *http://www.osti.gov/bridge/product.biblio.jsp?osti_id=981926*

Kenisarin, M. M. (2010), 'High-temperature phase change materials for thermal energy storage', *Renewable and Sustainable Energy Reviews* **14**(3), 955–970.
**URL:** *http://linkinghub.elsevier.com/retrieve/pii/S1364032109002731*

Kolb, G. J. (2011), An Evaluation of Possible Next-Generation High-Temperature Molten-Salt Power Towers, Technical Report December, Sandia National Laboratories, Albuquerque.
**URL:** *http://prod.sandia.gov/techlib/access-control.cgi/2011/119320.pdf*

Koll, G., Sahraoui, T., Hoffschmidt, B., Khedim, A., Pomp, S., Schwarzbözl, P. and Dillig, M. (2011), ALSOL Solar Thermal Tower Power Plant Algeria, *in* 'SolarPACES 2011', number august 2009, Granada, Spain.

Kopp, J. E. (2009), Two-Tank Indirect Thermal Storage Designs for Solar Parabolic Trough Power Plants, Msc., University of Nevada, Las Vegas.
**URL:** *http://link.aip.org/link/ASMECP/v2009/i48906/p683/s1&Agg=doi*

Kotzé, J. P., Backström, T. W. V. and Erens, P. J. (2012*a*), Evaluation of a latent heat thermal energy storage system using AlSi12 as a phase change material, *in* 'SolarPACES 2012', Marrakech, Morocco.

Kotzé, J. P., Backström, T. W. V. and Erens, P. J. (2012*b*), NaK as a primary heat transfer fluid in thermal solar power installations, *in* '1st Southern African Solar Energy Conference', Stellenbosch, South Africa.

Kotzé, J. P., von Backström, T. W. and Ehrens, P. J. (2012), NaK as a Primary Heat Transfer Fluid in Thermal Solar Power Installations, *in* '1st Southern African Solar Energy Conference', Stellenbosch, South Africa.

Kulhánek, M. and Dostál, V. (2011), Thermodynamic Analysis and Comparison of Supercritical Carbon Dioxide Cycles, *in* 'Supercritical CO2 Power Cycle Symposium', Boulder, CO, pp. 2–8.

Laing, D., Bahl, C., Bauer, T., Fiss, M., Breidenbach, N. and Hempel, M. (2012), High-Temperature Solid-Media Thermal Energy Storage for Solar Thermal Power Plants, *in* 'Proceedings of the IEEE', Vol. 100, pp. 516–524.

Laing, D., Bahl, C., Bauer, T., Lehmann, D. and Steinmann, W.-D. (2011), 'Thermal energy storage for direct steam generation', *Solar Energy* **85**(4), 627–633.
**URL:** *http://www.sciencedirect.com/science/article/pii/S0038092X10002835*

Laing, D., Bauer, T., Lehmann, D. and Bahl, C. (2010), 'Development of a Thermal Energy Storage System for Parabolic Trough Power Plants With Direct Steam Generation', *Journal of Solar Energy Engineering* **132**(2), 21011–21018.
**URL:** *http://dx.doi.org/10.1115/1.4001472*

Laing, D., Eck, M., Hempel, M., Johnson, M., Steinmann, W.-D., Meyer, M. and Eickhoff, M. (2012), High Temperature PCM Storage for DSG Solar Thermal Power Plants

Tested in Various Operating Modes of Water/Steam Flow, *in* 'SolarPACES 2012', Marrakech, Morocco.

Laing, D., Steinmann, W.-D., Fiss, M., Tamme, R., Brand, T., Bahl, C. and Fiß, M. (2008), 'Solid Media Thermal Storage Development and Analysis of Modular Storage Operation Concepts for Parabolic Trough Power Plants', *Journal of Solar Energy Engineering* **130**(1), 011006.
**URL:** *http://link.aip.org/link/JSEEDO/v130/i1/p011006/s1&Agg=doi*

Laing, D., Steinmann, W.-D., Tamme, R. and Richter, C. (2006), 'Solid media thermal storage for parabolic trough power plants', *Solar Energy* **80**(10), 1283–1289.
**URL:** *http://linkinghub.elsevier.com/retrieve/pii/S0038092X06001538*

Lata, J. M., Rodriguez, M. and de Lara, M. A. (2008), 'High Flux Central Receivers of Molten Salts for the New Generation of Commercial Stand-Alone Solar Power Plants', *Journal of Solar Energy Engineering* **130**(2), 021002.
**URL:** *http://link.aip.org/link/JSEEDO/v130/i2/p021002/s1&Agg=doi*

Lemmon, E. W., McLinden, M. O. and Friend, D. G. (2011), NIST Chemistry WebBook, *in* P. J. Linstrom and W. G. Mallard, eds, 'NIST Standard Reference Database Number 69', Gaithersburg, MD.
**URL:** *http://webbook.nist.gov*

Li, P. W., Lew, J. V., Karaki, W., Chan, C. L., Stephens, J. and Brien, J. E. O. (2011), Transient Heat Transfer and Energy Transport in Packed Bed Thermal Storage Systems, *in* M. A. D. S. Bernardes, ed., 'Developments in Heat Transfer', InTech, chapter 20, pp. 373–416.
**URL:** *http://www.intechopen.com/books/developments-in-heat-transfer/transient-heat-transfer-and-energy-transport-in-packed-bed-thermal-storage-systems*

Litwin, R. Z. (2002), Receiver System: Lessons Learned from Solar Two, Technical Report March, Sandia National Laboratories, Canoga Park, CA.
**URL:** *http://prod.sandia.gov/techlib/access-control.cgi/2002/020084.pdf*

Liu, M., Saman, W. and Bruno, F. (2012), 'Review on storage materials and thermal performance enhancement techniques for high temperature phase change thermal storage systems', *Renewable and Sustainable Energy Reviews* **16**(4), 2118–2132.
**URL:** *http://www.sciencedirect.com/science/article/pii/S1364032112000214*

Ma, Z. and Turchi, C. S. (2011), Advanced Supercritical Carbon Dioxide Power Cycle Configurations for Use in Concentrating Solar Power Systems, *in* 'Supercritical CO2 Power Cycle Symposium', number March, Boulder.

Mann, D., Field, R. E. and Viskanta, R. (1992), 'Determination of specific heat and true thermal conductivity of glass from dynamic temperature data', *Wärme - und Stoffübertragung* **27**(4), 225–231.
**URL:** *http://dx.doi.org/10.1007/BF01589920*

Massidda, L. and Varone, A. (2007), A Numerical Analysis of a High Temperature Solar Collecting Tube, Using Helium as an Heat Transfer Fluid, Technical report, CRS4, Pula, Italy.
**URL:** *http://publications.crs4.it/pubdocs/2007/MV07c/crs4_1180.pdf*

Medrano, M., Gil, A., Martorell, I., Potau, X. and Cabeza, L. F. (2010), 'State of the art on high-temperature thermal energy storage for power generation. Part 2 - Case studies', *Renewable and Sustainable Energy Reviews* **14**(1), 56–72.
**URL:** *http://linkinghub.elsevier.com/retrieve/pii/S1364032109001786*

Mertins, M. (2009), Technische und wirtschaftliche Analyse von horizontalen Fresnel-Kollektoren, Dissertation, Technische Universtät Karlsruhe.
**URL:** *http://digbib.ubka.uni-karlsruhe.de/volltexte/1000013884*

Michels, H. and Pitz-Paal, R. (2007), 'Cascaded latent heat storage for parabolic trough solar power plants', *Solar Energy* **81**(6), 829–837.
**URL:** *http://linkinghub.elsevier.com/retrieve/pii/S0038092X06002398*

Moisseytsev, A. and Sienicki, J. J. (2010), Extension of the Supercritical Carbon Dioxide Brayton Cycle for Application to the Very High Temperature Reactor, *in* 'Proceedings of ICAPP '10', San Diego, CA.

Moore, R., Vernon, M., Ho, C. K., Siegel, N. P. and Kolb, G. J. (2010), Design Considerations for Concentrating Solar Power Tower Systems Employing Molten Salt, Technical Report September, Sandia National Laboratories.
**URL:** *prod.sandia.gov/techlib/access-control.cgi/2010/106978.pdf*

Morita, K., Maschek, W., Flad, M., Yamano, H. and Tobita, Y. (2006), 'Thermophysical Properties of Lead-Bismuth Eutectic Alloy in Reactor Safety Analyses', *Journal of Nuclear Science and Technology* **43**(5), 526–536.
**URL:** *http://www.tandfonline.com/doi/abs/10.1080/18811248.2006.9711131*

Muto, Y. and Kato, Y. (2007), Optimal Cycle Scheme of Direct Cycle Supercritical CO 2 Gas Turbine for Nuclear Power Generation Systems, *in* 'International Conference of Power Engineering 2007', Hangzhou, China, pp. 86–92.

Novatec Solar (2013), 'Projects'.
**URL:** *http://novatecsolar.com/*

NREL (2013*a*), 'Concentrating Solar Power Projects'.
**URL:** *http://www.nrel.gov/csp/solarpaces/by_technology.cfm*

NREL (2013*b*), 'Ivanpah Solar Energy Generating System'.
**URL:** *http://www.nrel.gov/csp/solarpaces/project_detail.cfm/projectID=62*

Olson, L. C., Ambrosek, J. W., Sridharan, K., Anderson, M. H. and Allen, T. R. (2009), 'Materials corrosion in molten LiFNaFKF salt', *Journal of Fluorine Chemistry* **130**(1), 67–73.
**URL:** *http://www.sciencedirect.com/science/article/pii/S002211390800119X*

Pacheco, J. E. and Dunkin, S. R. (1996), Assessment of Molten-Salt Solar Central-Receiver Freeze-Up and Recovery Events, Technical report, Sandia National Laboratories, Albuquerque.
**URL:** *http://www.osti.gov/bridge/servlets/purl/202442-mwiLFH/webviewable/202442.pdf*

Pacheco, J. E., Reilly, H. E. and Gregory, J. (2000), Summary of the solar two test and evaluation program, Technical report, Sandia National Laboratories.
**URL:** *http://www.stratosolar.com/uploads/5/6/7/1/5671050/23_solar_2_test_and_evaluation_751185.pdf*

Pacheco, J. E., Showalter, S. K. and Kolb, W. J. (2002), 'Development of a Molten-Salt Thermocline Thermal Storage System for Parabolic Trough Plants', *Journal of Solar Energy Engineering* **124**(2), 153–159.
**URL:** *http://dx.doi.org/10.1115/1.1464123*

Pacio, J. and Wetzel, T. (2013), 'Assessment of liquid metal technology status and research paths for their use as efficient heat transfer fluids in solar central receiver systems', *Solar Energy* **93**, 11–22.
**URL:** *http://linkinghub.elsevier.com/retrieve/pii/S0038092X13001357*

Pilkington Solar International GmbH (2000), Survey of Thermal Storage for Parabolic Trough Power Plants, Technical Report September, NREL, Golden, CO.

Poplavskii, V. M., Bagdasarov, Y. E., Kamaev, a. a., Tsikunov, A. G., Zybin, V. A. and Ivanenko, V. N. (2004), 'Danger of Burning of Sodium Coolant', *Atomic Energy* **96**(5), 327–331.
**URL:** *http://link.springer.com/10.1023/B:ATEN.0000038098.44375.1a*

Powell, K. M. and Edgar, T. F. (2012), 'Modeling and control of a solar thermal power plant with thermal energy storage', *Chemical Engineering Science* **71**(0), 138–145.
**URL:** *http://www.sciencedirect.com/science/article/pii/S0009250911008657*

Professorship of Renewable Energy Carriers (2013), 'Publications'.
**URL:** *http://www.pre.ethz.ch/publications/journals/*

Querol, P., Olano, J., Velasco, T. and Arevalo, J. E. (2012), Single tank thermal storage prototype, *in* 'SolarPACES 2012', Marrakech, Morocco.

Raade, J. W., Elkin, B. and Vaughn, J. (2012), Novel 700 C Molten Salt for Solar Thermal Power Generation with Supercritical Steam Turbines, *in* 'SolarPACES 2012', Vol. 001, Marrakech, Morocco.

Raade, J. W. and Padowitz, D. (2011), 'Development of Molten Salt Heat Transfer Fluid With Low Melting Point and High Thermal Stability', *Journal of Solar Energy Engineering* **133**(3), 31013–31016.
**URL:** *http://dx.doi.org/10.1115/1.4004243*

Reilly, H. E. and Kolb, G. J. (2001), An Evaluation of Molten-Salt Power Towers Including Results of the Solar Two Project, Technical report, Sandia National Laboratories.
**URL:** *http://www.osti.gov/energycitations/product.biblio.jsp?osti_id=791898*

Robak, C. W., Bergman, T. L. and Faghri, A. (2011), 'Economic evaluation of latent heat thermal energy storage using embedded thermosyphons for concentrating solar power applications', *Solar Energy* **85**(10), 2461–2473.
**URL:** *http://www.sciencedirect.com/science/article/pii/S0038092X11002489*

Rodríguez-Sanchez, M. R., Venegas-Bernal, M., Marugán-Cruz, C. and Santana, D. (2013), Thermal, mechanical and hydrodynamic analysis to optimize the design of molten salt central receivers of solar tower power plants., *in* 'International Conference on Renewable Energies and Power Quality', number 11, Bilbao.
**URL:** *http://www.icrepq.com/icrepq%2713/238-rodriguez.pdf*

Rouillard, F., Charton, F. and Moine, G. (2009), Corrosion behaviour of different metallic materials in supercritical CO2 at 550 C and 250 bars, *in* 'Proceedings of SCCO2 Power Cycle Symposium 2009', Troy, NY.

Sabharwall, P., Ebner, M., Sharpe, P., Ambrosek, J., Anderson, M., Sridharan, K., Olson, L. and Brooks, P. (2010), Molten Salts for High Temperature Reactors : University of Wisconsin Molten Salt Corrosion and Flow Loop Experiments Issues Identified and Path Forward, Technical Report March, Idaho National Laboratory, Idaho Falls, ID.
**URL:** *www.inl.gov/technicalpublications/Documents/4502649.pdf*

Schiel, W. J. C. and Geyer, M. A. (1988), 'Testing an external sodium receiver up to heat fluxes of 2.5 MW/m2: Results and conclusions from the IEA-SSPS high flux experiment conducted at the central receiver system of the Plataforma Solar de Almeria (Spain)', *Solar Energy* **41**(3), 255–265.
**URL:** *http://www.sciencedirect.com/science/article/pii/0038092X88901430*

Schneider, G., Maier, H. and Stenglein, M. (2011), Development of large scale High Temperature Thermal Energy Storage System ( HTTESS ) for CSP-power plants, *in* 'SolarPACES 2011', Granada, Spain.

Schwaiger, K., Haider, M., Walter, H., Puigpinos, M. and Proetsch, A. (2012), Thermal Storage of Superheated Steam in a Combined Sensible/Latent TES, *in* 'SolarPACES 2012', Marrakech, Morocco.

Schwarzbözl, P., Buck, R., Sugarmen, C., Ring, A., Marcos Crespo, M. J., Altwegg, P. and Enrile, J. (2006), 'Solar gas turbine systems: Design, cost and perspectives', *Solar Energy* **80**(10), 1231–1240.
**URL:** *http://www.sciencedirect.com/science/article/pii/S0038092X05003348*

Selvam, R. P. and Strasser, M. N. (2012), Development of a Structured Thermocline Thermal Energy Storage System, *in* 'World Renewable Energy Forum', Denver, CO, pp. 1–17.

Sengers, J. V. and Watson, J. T. R. (1986), 'Improved International Formulations for the Viscosity and Thermal Conductivity of Water Substance', *Journal of Physical and Chemical Reference Data* **15**(4), 1291–1314.
**URL:** *http://www.nist.gov/data/PDFfiles/jpcrd303.pdf*

Shand, E. B. (1958), *Glass Engineering Handbook Second Edition*, 2nd edn, McGraw-Hill, York, PA.
**URL:** *http://www.amazon.com/Glass-Engineering-Handbook-Second-Edition/dp/B000OMIYDO*

Siegel, N. P., Bradshaw, R. W., Cordaro, J. B. and Kruizenga, A. M. (2011), 'Thermophysical Property Measurement of Nitrate Salt Heat Transfer Fluids', *ASME Conference Proceedings* **2011**(54686), 439–446.
**URL:** *http://dx.doi.org/10.1115/ES2011-54058*

SIEMENS AG (2010), 'Steam turbines for CSP plants'.
**URL:** *http://www.siemens.com/sustainability/pool/de/umweltportfolio/produkteloesungen/energieuebertragung-energieverteilung/solar-energy_steam-turbines.pdf*

SIEMENS AG (2012), 'Industrial Steam Turbines'.
**URL:** *http://www.energy.siemens.com/hq/pool/hq/power-generation/steamturbines/Industrial_Steam_Turbines_en.pdf*

Sienicki, J. J., Moisseytsev, A., Fuller, R. L., Wright, S. A. and Pickard, P. S. (2011), Scale Dependencies of Supercritical Carbon Dioxide Brayton Cycle Technologies and the Optimal Size for a Next-Step Supercritical CO2 Cycle Demonstration, *in* 'SCO2 Power Cycle Symposium', Boulder, CO.
**URL:** *http://www.sco2powercyclesymposium.org/resource_center/development_priorities/scale-dependencies-of-supercritical-carbon-dioxide-brayton-cycle-technologies-and-the-optimal-size-for-a-next-step-supercritical-co2-cycle-demonstration*

Singer, C., Buck, R., Pitz-Paal, R. and Muller-Steinhagen, H. (2010), 'Assessment of Solar Power Tower Driven Ultrasupercritical Steam Cycles Applying Tubular Central Receivers With Varied Heat Transfer Media', *Journal of Solar Energy Engineering* **132**(4).
**URL:** *http://link.aip.org/link/JSEEDO/v132/i4/p041010/s1&Agg=doi*

Solúcar (2006), Final Technical Progress Report, Technical Report November 2006.

Solugas Consortium (2012), 'Solugas - Solar Up-scale Gas Turbine System'.
**URL:** *http://www.solugas.com/index/index.php*

Solutia Inc. (2013), 'Therminol VP-1 Vapor Phase/Liquid Phase Heat Transfer Fluid'.
**URL:** *http://www.therminol.com/pages/products/eu/vp-1.asp*

Spelling, J., Guédez, R. and Laumert, B. (2012), The Value of Storage in Hybrid Solar Gas-Turbine Power Plants, *in* 'SolarPACES 2012', Marrakech, Morocco.

Steinmann, W.-D. and Eck, M. (2006), 'Buffer storage for direct steam generation', *Solar Energy* **80**(10), 1277–1282.
**URL:** *http://linkinghub.elsevier.com/retrieve/pii/S0038092X05002203*

Tamme, R., Laing, D. and Steinmann, W.-D. (2003), 'Advanced Thermal Energy Storage Technology for Parabolic Trough', *Solar Energy* (March), 563–571.
**URL:** *http://link.aip.org/link/ASMECP/v2003/i36762/p563/s1&Agg=doi*

Tian, Y. and Zhao, C. Y. (2013), 'A review of solar collectors and thermal energy storage in solar thermal applications', *Applied Energy* **104**(0), 538–553.
**URL:** *http://www.sciencedirect.com/science/article/pii/S0306261912008549*

Turchi, C. S. (2009), Supercritical CO2 for Application in Concentrating Solar Power Systems, *in* 'Proceedings of SCCO2 Power Cycle Symposium 2009', number Figure 1, Troy, NY, pp. 1–5.
**URL:** *http://www.sco2powercyclesymposium.org/resource_center/system_concepts/supercritical-co2-for-application-in-concentrating-solar-power-systems*

Turkdogan, E. T. (1983), *Physicochemical properties of molten slags and glasses*, Metals Society, London, UK.
**URL:** *http://books.google.co.za/books/about/Physicochemical_properties_of_molten_sla.html?id=TzhRAAAAMAAJ&pgis=1*

Tyner, C. E., Sutherland, J. P. and Gould, W. R. J. (1995), Solar Two: A Molten Salt Power Tower Demonstration, Technical report, Sandia National Laboratories.
**URL:** *large.stanford.edu/publications/coal/references/docs/1605696.pdf*

U.S. Department of Energy (2012*a*), 'Advanced Heat Transfer Fluids and Novel Thermal Storage Concepts for CSP Generation'.
**URL:** *http://www1.eere.energy.gov/solar/sunshot/csp_storage_awards.html*

U.S. Department of Energy (2012*b*), 'High Operating Temperature Liquid Metal Heat Transfer Fluids'.
**URL:** *http://www1.eere.energy.gov/solar/sunshot/muri_ucla.html*

Van Lew, J. T., Li, P., Chan, C. L., Karaki, W. and Stephens, J. (2011), 'Analysis of Heat Storage and Delivery of a Thermocline Tank Having Solid Filler Material', *Journal of Solar Energy Engineering* **133**(2), 2100301–210310.
**URL:** *http://dx.doi.org/10.1115/1.4003685*

Wagner, M. J. (2008), Simulation and Predictive Performance Modeling of Utility-Scale Central Receiver System Power Plants by, Msc, University of Wisconsin - Madison.
**URL:** *http://sel.me.wisc.edu/publications/theses/wagner08.zip*

Weitzel, P. S. (2011), Steam Generator for Advanced Ultra-Supercritical Power Plants 700 to 760C, *in* 'ASME 2011 Power Conference', Denver, CO.
**URL:** *www.babcock.com/library/pdf/br-1852.pdf*

Williams, D. F. (2006), Assessment of Candidate Molten Salt Coolants for the NGNP/NHI Heat-Transfer Loop, Technical Report June, Oak Ridge National Laboratory, Oak Ridge.
**URL:** *https://inlportal.inl.gov/portal/server.pt/gateway/PTARGS_0_2_3310_277_2604_43/http;/inlpublisher;7087/publishedcontent/publish/communities/inl_gov/about_inl/gen_iv___technical_documents/ornl_tm_2006_69_htl_salt.pdf*

Wilson Solarpower (2010*a*), 'Core Technology'.
**URL:** *http://wilsonsolarpower.com/index.php/solution/coretechnology.html*

Wilson Solarpower (2010*b*), 'Wilson Heat Exchanger'.
**URL:** *http://wilsonsolarpower.com/index.php/nonsolarapps/77-wilsonheatexchanger.html*

Wright, S. A., Conboy, T. M., Parma, E. J., Tom G. Lewis, Gary A. Rochau and Ahti J. Suo-Anttila (2011), Summary of the Sandia Supercritical CO2 Development Program, *in* 'SCO2 Power Cycle Symposium', Boulder, CO.

Wright, S. A., Conboy, T. M. and Rochau, G. E. (2011), 'Overview of supercritical CO2 power cycle development at sandia national laboratories'.

Wu, W., Gobereit, B., Singer, C., Amsbeck, L. and Pitz-Paal, R. (2011), Direct Absorption Receivers for High Temperatures, *in* 'SolarPACES 2011', Granada, Spain.
**URL:** *http://elib.dlr.de/73113/*

Xu, C., Wang, Z., He, Y., Li, X. and Bai, F. (2012), 'Parametric study and standby behavior of a packed-bed molten salt thermocline thermal storage system', *Renewable Energy* **48**(0), 1–9.
**URL:** *http://www.sciencedirect.com/science/article/pii/S0960148112002583*

Yang, M., Yang, X., Yang, X. and Ding, J. (2010), 'Heat transfer enhancement and performance of the molten salt receiver of a solar power tower', *Applied Energy* **87**(9), 2808–2811.
**URL:** *http://www.sciencedirect.com/science/article/pii/S0306261909001834*

Yang, Z. and Garimella, S. V. (2010), 'Molten-salt thermal energy storage in thermoclines under different environmental boundary conditions', *Applied Energy* **87**(11), 3322–3329.
**URL:** *http://www.sciencedirect.com/science/article/pii/S0306261910001315*

Yogev, R. and Kribus, A. (2012), Performance of Solar Thermal Power Plants Operating from PCM Storage, *in* 'SolarPACES 2012', Marrakech, Morocco.

Zalba, B., Marn, J. M., Cabeza, L. F. and Mehling, H. (2003), 'Review on thermal energy storage with phase change: materials, heat transfer analysis and applications', *Applied Thermal Engineering* **23**, 251–283.
**URL:** *http://linkinghub.elsevier.com/retrieve/pii/S1359431102001928*

Zanganeh, G., Pedretti, A., Zavattoni, S., Barbato, M. and Steinfeld, A. (2012), 'Packed-bed thermal storage for concentrated solar power Pilot-scale demonstration and industrial-scale design', *Solar Energy* **86**(10), 3084–3098.
**URL:** *http://www.sciencedirect.com/science/article/pii/S0038092X12002812*

Zavattoni, S. A., Barbato, M. C., Pedretti, A. and Zanganeh, G. (2011), CFD Simulation of a Pebble Bed Thermal Energy Storage System Accounting for Porosity Variations Effects, *in* 'SolarPACES 2011', Granada, Spain.

Zaversky, F., Medina, R., García-barberena, J., Sánchez, M. and Astrain, D. (2012), Part Load Behavior of Oil-to-Molten-Salt Heat Exchanger Configurations for Active Indirect Storage Systems in CSP Applications, *in* 'SolarPACES 2012', Marrakech, Morocco.

Zavoico, A. B. (2001), Solar Power Tower Design Basis Document, Technical Report July, Sandia National Laboratories.
**URL:** *http://prod.sandia.gov/techlib/access-control.cgi/2001/012100.pdf*

Zhang, J. and Li, N. (2008), 'Review of the studies on fundamental issues in LBE corrosion', *Journal of Nuclear Materials* **373**(13), 351–377.
**URL:** *http://www.sciencedirect.com/science/article/pii/S0022311507008422*

Zhao, C. Y. and Wu, Z. G. (2011), 'Thermal property characterization of a low melting-temperature ternary nitrate salt mixture for thermal energy storage systems', *Solar Energy Materials and Solar Cells* **95**(12), 3341–3346.
**URL:** *http://www.sciencedirect.com/science/article/pii/S0927024811004478*

Zipf, V., Neuhäuser, A., Willert, D., Nitz, P., Gschwander, S. and Platzer, W. (2012), 'High temperature latent heat storage with a screw heat exchanger: Design of prototype', *Applied Energy* (0).
**URL:** *http://www.sciencedirect.com/science/article/pii/S0306261912008471*

Zunft, S., Hahn, J. and Kammel, J. (2011), Flow Distribution Calculations in Regenerator-Type Heat Storage for Solar Tower Plants, *in* 'SolarPACES 2011', Granada, Spain.

Zunft, S., Hänel, M., Krüger, M., Dreißigacker, V., Göhring, F. and Wahl, E. (2011), 'Jülich Solar Power Tower - Experimental Evaluation of the Storage Subsystem and Performance Calculation', *Journal of Solar Energy Engineering* **133**(3), 31015–31019.
**URL:** *http://link.aip.org/link/?SLE/133/031019/1*

# Appendix

## A. Properties of HTFs

### A.1. Overview

| Property | Unit | Synthetic Oil | *Solar Salt*™ | *HITEC*® *Heat Transfer Salt* | Low-T Salt (KLiNa/$NO_2$,$NO_3$) | High-T Salt1 (LiF-NaF-KF) | High-T Salt2 (Saltstream™ 700) | Na | NaK | LBE |
|---|---|---|---|---|---|---|---|---|---|---|
| $T_{min}$ | ℃ | 15 | 222 | 142 | 75 | 454 | 253 | 97.7 | -12.6 | 125 |
| $T_{min,pract}$ | ℃ | 292 | 290 | 142 | 75 | 500 | 300 | 285 | 285 | 285 |
| $T_{max,pract}$ | ℃ | 393 | 593 | 538 | 550 | 1000 | 700 | 873 | 785 | 1670 |
| corresponding pressures | bar | 11 | 1–20 | n.a. | | 1 | 1 | 1 | 1 | 1 |
| $\rho$ | kg/m$^3$ | 815–673 | 1910–1720 | 1980–1690 | | 2200–1800 | 2270–2040 | 884–745 | 779–659 | 10 300–8770 |
| $c_p$ | kJ/kg K | 2.37–2.73 | 1.49–1.55 | 1.40–0.95 | | 1.89 (@700 °C) | 1.45 (@ 300 °C) | 1.31–1.27 | 0.893–(0.872–)0.892 | 0.146–0.114 |
| $\lambda$ | W/m K | 0.0953–0.0771 | 0.50–0.55 | 0.44–0.24 | | 0.60–1.00 | | 76.3–49.0 | 25.5–26.3–24.1 | 12.5–26.6 |
| $\mu$ | mPa s | 0.25–0.12 | 3.50–1.03 | 20.0–1.00 | | 12.4–1.06 | 8.4 (@ 400 °C); 4.2 (@ 500 °C) | 0.35–0.16 | 0.279–0.131 | 1.91–0.725 |
| cost[a] | USD/kg | 2.10 | 0.70–0.93 | 0.80 | | 11.30 | | 2.00 | 2.00 | 13.00 |
| storage implementation | | - | + | + | + | o | o | o | o | o |
| HTF also working fluid | | - | - | - | - | - | - | -/+[b] | - | - |

[a] for reference of cost information, see following tables
[b] AMTEC, see Section 3.3.1

| Property | Unit | ambient Air | pressurized Air | DSG-superheated | s-$H_2O$ (USC) | s-$CO_2$ |
|---|---|---|---|---|---|---|
| $T_{min}$ | ℃ | n.a. | n.a. | 0 | 0 | n.a. |
| $T_{min,pract}$ | ℃ | 100 | 100 | 249 | 300 | 32 |
| $T_{max,pract}$ | ℃ | 1300 | 1000 for reference | 600 | 620 | 850 |
| corresponding pressure(s) | bar | 1 | 20 | 190 | 240 | 78–200 |
| $\rho$ | kg/m$^3$ | 0.934–0.222 | 18.7–5.47 | 815–52.0 | 741–65.1 | 881–36.1 |
| $c_p$ | kJ/kg K | 1.02–1.22 | 1.02–1.19 | 4.19–10.4–2.76 | (5600–)5.21–2.86 | (54.3–)1.28–2.17 |
| $\lambda$ | W/m K | 0.0314–0.0966 | 0.0321–0.0818 | 0.634–0.0952 | 0.578–0.10466 | 0.07–0.103 |
| $\mu$ | mPa s | 0.0219–0.0582 | 0.0221–0.0509 | 0.110–0.0338 | 0.0914–0.0351 | (0.087–)0.0450–0.0477 |
| cost[c] | USD/kg | 0 | 0 | | | |
| storage implementation | | o | - | - | - | - |
| HTF also working fluid | | - | + | + | + | + |

[c] for reference of cost information, see following tables

## A.2. Synthetic Oil Therminol® VP-1/Dowtherm® A

Table 3: Detailed HTF Properties - Synthetic Oil

| Property | Unit | | |
|---|---|---|---|
| $T_{\min}$ (freeze protection) | °C | 15 | Dow Chemical Company (2001) |
| lower operating $T$ (reference for below) | °C | 292 | Feldhoff et al. (2012) |
| practical $T_{\max}$ (reference for below) | °C | 393 | Dow Chemical Company (2001) |
| corresponding pressure(s) | bar | 11 | Dow Chemical Company (2001) |
| density range $\rho$ | kg/m$^3$ | 815–673 | Dow Chemical Company (2001) |
| isobaric specific heat capacity $c_\mathrm{p}$ | kJ/kg K | 2.37–2.73 | Dow Chemical Company (2001) |
| th. Conductivity $\lambda$ | W/m K | 0.0953–0.0771 | Dow Chemical Company (2001) |
| dyn. Viscosity $\mu$ | mPa s | 0.25–0.12 | Dow Chemical Company (2001) |
| cost (2011) | USD/kg | 2.10 | Robak et al. (2011) |
| storage implementation | | - | |
| also working fluid? | | - | |
| comments | | state of the art | |

Correlations (Kopp, 2009):

$$\lambda_\mathrm{oil} = \left[0.1381 - 0.00008708\ t/°\mathrm{C} - 0.0000001729\ (t/°\mathrm{C})^2\right] \mathrm{W/m\,K}$$

$$c_\mathrm{p,oil} = \left[1.509 + 0.002496\ t/°\mathrm{C} + 0.0000007888\ (t/°\mathrm{C})^2\right] \mathrm{kJ/kg\,K}$$

## A.3. Solar Salt™

Table 4: Detailed HTF Properties - *HITEC® Solar Salt™*

| Property | Unit | | |
|---|---|---|---|
| $T_{\min}$ (freeze protection) | °C | 222 | Coastal Chemical Co. (n.d.*b*) |
| lower operating $T$ (reference for below) | °C | 290 | Gemasolar (2011) |
| practical $T_{\max}$ (reference for below) | °C | 593 | Coastal Chemical Co. (n.d.*b*) |
| corresponding pressures | bar | 1–20 | Kelly (2010) |
| density range $\rho$ | kg/m$^3$ | 1910–1720 | Wagner (2008) |
| isobaric specific heat capacity $c_\mathrm{p}$ | kJ/kg K | 1.49–1.55 | Wagner (2008) |
| th. Conductivity $\lambda$ | W/m K | 0.50–0.55 | Wagner (2008) |
| dyn. Viscosity $\mu$ | mPa s | 3.50–1.03 | Wagner (2008) |
| cost (2012) | USD/kg | 0.50 | Pacio and Wetzel (2013) |
| storage implementation | | + | |
| HTF also working fluid | | - | |
| comments | | | |

Correlations (Kopp, 2009), based on Wagner (2008):

$$\lambda_\mathrm{solarsalt} = \left[0.443 + 0.00019\ t/°\mathrm{C}\right] \mathrm{W/m\,K}$$

$$c_\mathrm{p,solarsalt} = \left[1.443 + 0.000172\ t/°\mathrm{C})\right] \mathrm{kJ/kg\,K}$$

$$\mu_\mathrm{solarsalt} = \left[22.714 - 0.12\ t/°\mathrm{C} + 0.0002281\ (t/°\mathrm{C})^2 - 0.0000001474\ (t/°\mathrm{C})^3\right] \mathrm{mPa\,s}$$

## A.4. HITEC® Heat Transfer Salt

Table 5: Detailed HTF Properties - *HITEC® Heat Transfer Salt*

| Property | Unit | | |
|---|---|---|---|
| $T_{\min}$ (freeze protection) | °C | 142 | Coastal Chemical Co. (n.d.*a*) |
| lower operating $T$ (reference for below) | °C | 142 | |
| practical $T_{\max}$ (reference for below) | °C | 538 | Coastal Chemical Co. (n.d.*a*) |
| corresponding pressures | bar | n.a. | |
| density range $\rho$ | kg/m$^3$ | 1980–1690 | Coastal Chemical Co. (n.d.*a*) |
| isobaric specific thermal capacity $c_p$ | kJ/kg K | 1.40–0.95 | Boerema et al. (2012) |
| th. Conductivity $\lambda$ | W/m K | 0.44–0.24 | Coastal Chemical Co. (n.d.*a*) |
| dyn. Viscosity $\mu$ | mPa s | 20.0–1.00 | Coastal Chemical Co. (n.d.*a*) |
| cost (2001/2002) | USD/kg | 0.70–0.93 | Kearney (2001) Herrmann and Kearney (2002) |
| storage implementation | | + | |
| HTF also working fluid | | - | |
| comments | | alternative to Solar Salt for linear systems because of lower $T_{melt}$ | |

Correlations (Flueckiger et al., 2011*a*):

$$\rho_{\text{HITEC}} = 1938 - 0.732\ (T/\text{K} - 200)$$

$$\mu_{\text{HITEC}} = 1000\ \Big[\exp\big(-4.343 - 2.0143\ (\ln(T/\text{K}) - 5.011)\big)\Big]\,\text{mPa s}$$

$$\lambda_{\text{HITEC}} = \big[-0.000653\ (T/\text{K} - 260) + 0.4210\big]\,\text{W/m K}$$

## A.5. Low Temperature Salt

Table 6: Detailed HTF Properties - Low Temperature Salts (KLiNa/$NO_2$,$NO_3$)

| Property | Unit | | |
|---|---|---|---|
| midrule $T_{min}$ (freeze protection) | ℃ | 75 | Bauer et al. (2012) |
| lower operating $T$ (reference for below) | ℃ | 75 | Bauer et al. (2012) |
| practical $T_{max}$ (reference for below) | ℃ | 550 | Bauer et al. (2012) |
| corresponding pressures | bar | | |
| density range $\rho$ | kg/m$^3$ | | |
| isobaric specific thermal capacity $c_p$ | kJ/kg K | | |
| th. Conductivity $\lambda$ | W/m K | | |
| dyn. Viscosity $\mu$ | mPa s | | |
| cost | USD/kg | | |
| storage implementation | | + | |
| HTF also working fluid | | - | |
| comments | | under development | |

## A.6. High Temperature Salts

Table 7: Detailed HTF Properties - LiF-NaF-KF

| Property | Unit | | |
|---|---|---|---|
| $T_{\min}$ (freeze protection) | ℃ | 454 | Forsberg et al. (2007) |
| lower operating $T$ (reference for below) | ℃ | 500 | Forsberg et al. (2007) |
| practical $T_{\max}$ (reference for below) | ℃ | 1000 (for reference, $T_{\text{melt}} \approx 1610$) | Forsberg et al. (2007) |
| corresponding pressures | bar | 1 | Forsberg et al. (2007) |
| density range $\rho$ | kg/m$^3$ | 2200–1800 | Williams (2006) |
| isobaric specific thermal capacity $c_{\text{p}}$ | kJ/kg K | 1.89 (@ 700 °C) | Forsberg et al. (2007) |
| th. Conductivity $\lambda$ | W/m K | 0.60–1.00 | Forsberg et al. (2007) |
| dyn. Viscosity $\mu$ | mPa s | 12.4–1.06 | Forsberg et al. (2007) |
| cost (1971) | USD/kg | 11.30 | Williams (2006) |
| storage implementation | | o | |
| HTF also working fluid | | - | |
| comments | | under development; HTF cost too high for direct storage | |

Table 8: Detailed HTF Properties - Saltstream™ 700

| Property | Unit | | |
|---|---|---|---|
| $T_{min}$ (freeze protection) | ℃ | 253 | Raade et al. (2012) |
| lower operating $T$ (reference for below) | ℃ | 300 | Raade et al. (2012) |
| practical $T_{max}$ (reference for below) | ℃ | 700 | Raade et al. (2012) |
| corresponding pressures | bar | 1 | Raade et al. (2012) |
| density range $\rho$ | kg/m$^3$ | 2270–2040 | Halotechnics (2012) |
| isobaric specific thermal capacity $c_p$ | kJ/kg K | 1.45 (@ 300 °C) | Raade et al. (2012) |
| th. Conductivity $\lambda$ | W/m K | | |
| dyn. Viscosity $\mu$ | mPa s | 8.4 (@ 400 °C); 4.2 (@ 500 °C) | Raade et al. (2012) |
| cost | USD/kg | | |
| storage implementation | | o | |
| HTF also working fluid | | - | |
| comments | | Announced in Dec. 2012; HTF cost too high for direct storage | |

## A.7. Sodium

Table 9: Detailed HTF Properties - Sodium (Na)

| Property | Unit | | |
|---|---|---|---|
| $T_{\min}$ (freeze protection) | ℃ | 97.7 | Boerema et al. (2012) |
| lower operating $T$ (reference for below) | ℃ | 285 | Boerema et al. (2012) |
| practical $T_{\max}$ (reference for below) | ℃ | 873 | Boerema et al. (2012) |
| corresponding pressures | bar | 1 | Boerema et al. (2012) |
| density range $\rho$ | kg/m$^3$ | 884–745 | Boerema et al. (2012) |
| isobaric specific thermal capacity $c_p$ | kJ/kg K | 1.31–1.27 | Boerema et al. (2012) |
| th. Conductivity $\lambda$ | W/m K | 76.3–49.0 | Boerema et al. (2012) |
| dyn. Viscosity $\mu$ | mPa s | 0.35–0.16 | Boerema et al. (2012) |
| cost (2012) | USD/kg | 2.00 | Pacio and Wetzel (2013) |
| storage implementation | | o | |
| HTF also working fluid | | -/o | |
| comments | | could be used in direct conversion power cycles | Hering et al. (2012) |

Correlations (Boerema et al., 2012):

$$\lambda_{\mathrm{Na}} = \left[124.67 - 0.11381\ T/\mathrm{K} + 5.5226 \cdot 10^{-5}\ (T/\mathrm{K})^2 - 1.1842 \cdot 10^{-8}\ (T/\mathrm{K})^3\right] \mathrm{W/m\,K}$$

$$c_{\mathrm{p,Na}} = \left[1.6582 - 8.4790 \cdot 10^{-4}\ T/\mathrm{K} + 4.4541 \cdot 10^{-7}\ (T/\mathrm{K})^2 - 2992.6\ (T/\mathrm{K})^{-2}\right] \mathrm{kJ/kg\,K}$$

$$\rho_{\mathrm{Na}} = \left[219 + 275.32\ (1 - T/2503.7\ \mathrm{K}) + 511.58\ (1 - T/2503.7\ \mathrm{K})^{0.5}\right] \mathrm{kg/m^3}$$

$$\mu_{\mathrm{Na}} = \left[1000\ \exp(-6.4406 - 0.3958\ \log(T/\mathrm{K}) + 556.835\ \mathrm{K}/T)\right] \mathrm{mPa\,s}$$

Correlations (Foust, 1972):

$$\lambda_{\mathrm{Na}} = \left[91.8 - 0.049\ t/^{\circ}\mathrm{C}\right] \mathrm{W/m\,K}$$

$$\rho_{\mathrm{Na}} = 1000 \left[0.9501 - 2.2976 \cdot 10^{-4}\ t/^{\circ}\mathrm{C} - 1.46 \cdot 10^{-8}\ (t/^{\circ}\mathrm{C})^2 + 5.638 \cdot 10^{-12}\ (t/^{\circ}\mathrm{C})^3\right] \mathrm{kg/m^3}$$

$$\mu_{\mathrm{Na}} = \begin{cases} \left[0.1235\ (\rho_{\mathrm{Na}}/1000\frac{\mathrm{kg}}{\mathrm{m}^3})^{1/3}\ \exp\left(697\ (\rho_{\mathrm{Na}}/1000\frac{\mathrm{kg}}{\mathrm{m}^3}) \cdot \mathrm{K}/T\right)\right] \mathrm{mPa\,s} & \text{if } T \leq 500\,^{\circ}\mathrm{C}, \\ \left[0.0851\ (\rho_{\mathrm{Na}}/1000\frac{\mathrm{kg}}{\mathrm{m}^3})^{1/3}\ \exp\left(1040\ (\rho_{\mathrm{Na}}/1000\frac{\mathrm{kg}}{\mathrm{m}^3}) \cdot \mathrm{K}/T\right)\right] \mathrm{mPa\,s} & \text{if } T > 500\,^{\circ}\mathrm{C}, \end{cases}$$

## A.8. Eutectic Sodium-Potassium Alloy

Table 10: Detailed HTF Properties - Eutectic Sodium-Potassium Alloy (NaK-78)

| Property | Unit | | |
|---|---|---|---|
| $T_{\min}$ (freeze protection) | ℃ | -12.6 | Foust (1972) |
| lower operating $T$ (reference for below) | ℃ | 285 | Boerema et al. (2012) |
| practical $T_{\max}$ (reference for below) | ℃ | 785 | Foust (1972) |
| corresponding pressures | bar | 1 | Foust (1972) |
| density range $\rho$ | kg/m$^3$ | 779–659 | Foust (1972) |
| isobaric specific thermal capacity $c_\mathrm{p}$ | kJ/kg K | 0.893–0.872–0.892 | Foust (1972) |
| th. Conductivity $\lambda$ | W/m K | 25.5–26.3–24.1 | Foust (1972) |
| dyn. Viscosity $\mu$ | mPa s | 0.279–0.131 | Foust (1972) |
| cost (2012) | USD/kg | 2.00 | Pacio and Wetzel (2013) |
| storage implementation | | o | |
| HTF also working fluid | | - | |
| comments | | | |

Correlations (Foust, 1972):

$$\lambda_\mathrm{NaK} = \left[21.4 + 0.0207\ t/°\mathrm{C} - 2.2\cdot 10^{-5}\ (t/°\mathrm{C})^2\right]\mathrm{W/m\,K}$$

$$\rho_\mathrm{NaK} = 1/v_{NaK}$$

$$v_\mathrm{NaK} = 1.003\ (0.778\ v_\mathrm{K} + 0.222\ v_\mathrm{Na})$$

$$v_\mathrm{K} = \left[0.001/\left(0.8415 - 2.172\cdot 10^{-4}\ t/°\mathrm{C} - 2.70\cdot 10^{-8}\ (t/°\mathrm{C})^2 + 4.77\cdot 10^{-12}\ (t/°\mathrm{C})^3\right)\right]\mathrm{m^3/kg}$$

$v_\mathrm{Na} = 1/v_\mathrm{Na}$ (see Section A.7)

$$c_\mathrm{p,NaK} = 4.184\left[0.2320 - 8.82\cdot 10^{-5}\ (t/°\mathrm{C}) + 8.2\cdot 10^{-8}\ (t/°\mathrm{C})^2\right]\mathrm{kJ/kg\,K}$$

$$\mu_\mathrm{NaK} = \begin{cases} \left[0.116\ (\rho_\mathrm{NaK}/1000\frac{\mathrm{kg}}{\mathrm{m^3}})^{1/3}\ \exp\left(688\ (\rho_\mathrm{NaK}/1000\frac{\mathrm{kg}}{\mathrm{m^3}})\cdot \mathrm{K}/T\right)\right]\mathrm{mPa\,s} & \text{if } T \le 400\,°\mathrm{C}, \\ \left[0.082\ (\rho_\mathrm{NaK}/1000\frac{\mathrm{kg}}{\mathrm{m^3}})^{1/3}\ \exp\left(979\ (\rho_\mathrm{NaK}/1000\frac{\mathrm{kg}}{\mathrm{m^3}})\cdot \mathrm{K}/T\right)\right]\mathrm{mPa\,s} & \text{if } T > 400\,°\mathrm{C}, \end{cases}$$

## A.9. Eutectic Lead-Bismuth Alloy

Table 11: Detailed HTF Properties - Eutectic Lead-Bismuth Alloy (LBE)

| Property | Unit | | |
|---|---|---|---|
| $T_{\min}$ (freeze protection) | ℃ | 125 | Morita et al. (2006) |
| lower operating $T$ (reference for below) | ℃ | 285 | Boerema et al. (2012) |
| practical $T_{\max}$ (reference for below) | ℃ | 1670 | Morita et al. (2006) |
| corresponding pressures | bar | 1 | Morita et al. (2006) |
| density range $\rho$ | kg/m$^3$ | 10300–8770 | Morita et al. (2006) |
| isobaric specific thermal capacity $c_\mathrm{p}$ | kJ/kg K | 0.146–0.114 | Morita et al. (2006) |
| th. Conductivity $\lambda$ | W/m K | 12.5–26.6 | Morita et al. (2006) |
| dyn. Viscosity $\mu$ | mPa s | 1.91–0.725 | Morita et al. (2006) |
| cost (2012) | USD/kg | 13.00 | Pacio and Wetzel (2013) |
| storage implementation | | o | |
| HTF also working fluid | | - | |
| comments | | | |

Correlations (Morita et al., 2006):

$$\lambda_\mathrm{LBE} = \Big[6.854 + 1.018 \cdot 10^{-2}\ T/\mathrm{K}\Big]\,\mathrm{W/m\,K}$$

$$\rho_\mathrm{LBE} = \Big[10981.7 - 1136.9 \cdot 10^{-3}\ T/\mathrm{K}\Big]\,\mathrm{kg/m^3}$$

$$\mu_\mathrm{LBE} = 1000\Big[0.49 \cdot 10^{-3}\ \exp(760.1\mathrm{K}/T)\Big]\,\mathrm{mPa\,s\ for\ } 398\,\mathrm{K} < T < 1273\,\mathrm{K}$$

$$c_\mathrm{p,NaK} = \Big[(159 - 2.302 \cdot 10^{-2}\ T/\mathrm{K})/1000\Big]\,\mathrm{kJ/kg\,K\ for\ } 400\,\mathrm{K} < T < 1100\,\mathrm{K}$$

## A.10. Ambient Air

Table 12: Detailed HTF Properties - Ambient Air

| Property | Unit | | |
|---|---|---|---|
| $T_{\min}$ (freeze protection) | ℃ | n.a. | |
| lower operating $T$ (reference for below) | ℃ | 100 | |
| practical $T_{\max}$ (reference for below) | ℃ | n.a. (1300 for reference) | |
| corresponding pressures | bar | 1 | |
| density range $\rho$ | kg/m$^3$ | 0.934–0.222 | ideal gas |
| isobaric specific thermal capacity $c_\mathrm{p}$ | kJ/kg K | 1.02–1.22 | Cengel and Boles (2010) |
| th. Conductivity $\lambda$ | W/m K | 0.0314–0.0966 | Kadoya et al. (1985) |
| dyn. Viscosity $\mu$ | mPa s | 0.0219–0.0582 | Kadoya et al. (1985) |
| cost | USD/kg | 0 | |
| storage implementation | | o | |
| HTF also working fluid | | - | |
| comments | | advantage of open cycle: HTF impurities, e.g. through rock bed storage, not an issue | |

Correlations:

$\rho_\mathrm{air} = \frac{p_\mathrm{air}}{R_\mathrm{air} T_\mathrm{air}}$ Ideal gas law

$c_\mathrm{p,air} = \left[(0.9703+6.7898{\cdot}10^{-5}(T/\mathrm{K})+1.6576{\cdot}10^{-7}(T/\mathrm{K})^2-6.7863{\cdot}10^{-11}(T/\mathrm{K})^3\right]\mathrm{kJ/kg\,K}$ (Cengel and Boles, 2010)

$\lambda_\mathrm{air} = 0.0259778\left[C_1 T_r + C_{0.5} T_r^{0.5} + \sum_{i=0}^{-4} C_i T_r^i + \sum_{j=1}^{5} D_j \rho_r^j\right]\mathrm{W/m\,K}$ (Kadoya et al., 1985)

with $T_\mathrm{r} = T/132.5\,\mathrm{K}$; $\rho_\mathrm{r} = \rho/314.3\,\mathrm{kg/m^3}$; $C_1 = 0.239503$; $C_{0.5} = 0.00649768$; $C_0 = 1$; $C_{-1} = -1.92615$; $C_{-2} = 2.00383$; $C_{-3} = -1.07553$; $C_{-4} = 0.229414$; $D_1 = 0.402287$; $D_2 = 0.356603$; $D_3 = -0.163159$; $D_4 = 0.138059$; $D_5 = -0.0201725$

$\mu_\mathrm{air} = 0.0061609\left[A_1 T_\mathrm{r} + A_{0.5} T_\mathrm{r}^{0.5} + \sum_{i=0}^{-4} A_i T_\mathrm{r}^i + \sum_{j=1}^{5} B_j \rho_\mathrm{r}^j\right]\mathrm{mPa\,s}$ (Kadoya et al., 1985)

with $T_\mathrm{r} = T/132.5\,\mathrm{K}$; $\rho_\mathrm{r} = \rho/314.3\,\mathrm{kg/m^3}$; $C_1 = 0.239503$; $A_1 = 0.128517$; $A_{0.5} = 2.60661$; $A_0 = -1$; $A_{-1} = -0.709661$; $A_{-2} = 0.662534$; $A_{-3} = -0.197846$; $A_{-4} = 0.00770147$; $B_1 = 0.465601$; $B_2 = 1.26469$; $B_3 = -0.511425$; $B_4 = 0.274600$

## A.11. Pressurized Air

Table 13: Detailed HTF Properties - Pressurized Air

| Property | Unit | | |
|---|---|---|---|
| $T_{\min}$ (freeze protection) | ℃ | n.a. | |
| lower operating $T$ (reference for below) | ℃ | 100 | |
| practical $T_{\max}$ (reference for below) | ℃ | n.a. (1000 for reference) | EC (2005) |
| corresponding pressures | bar | 20 | |
| density range $\rho$ | kg/m$^3$ | 18.7–5.47 | ideal gas |
| isobaric specific thermal capacity $c_p$ | kJ/kg K | 1.02–1.19 | Cengel and Boles (2010) |
| th. Conductivity $\lambda$ | W/m K | 0.0321–0.0818 | Kadoya et al. (1985) |
| dyn. Viscosity $\mu$ | mPa s | 0.0221–0.0509 | Kadoya et al. (1985) |
| cost | USD/kg | 0 | |
| storage implementation | | - | |
| HTF also working fluid | | + | |
| comments | | advantage of open cycle: HTF impurities (e.g., through rock bed storage) not an issue | |

Correlations: see Section A.10

## A.12. DSG - Superheated

Table 14: Detailed HTF Properties - Superheated Direct Steam Generation

| Property | Unit | | |
|---|---|---|---|
| $T_{\text{min}}$ (freeze protection) | ℃ | 0 | |
| lower operating $T$ (reference for below) | ℃ | 249 | NREL (2013*b*) |
| practical $T_{\text{max}}$ (reference for below) | ℃ | 600 | SIEMENS AG (2012) |
| corresponding pressures | bar | 190 | SIEMENS AG (2012) |
| density range $\rho$ | kg/m$^3$ | 815–52.0 | Sengers and Watson (1986) |
| isobaric specific thermal capacity $c_{\text{p}}$ | kJ/kg K | 4.19–10.4–2.76 | Cengel and Boles (2010) |
| th. Conductivity $\lambda$ | W/m K | 0.634–0.0952 | Sengers and Watson (1986) |
| dyn. Viscosity $\mu$ | mPa s | 0.110–0.0338 | Sengers and Watson (1986) |
| cost | USD/kg | | Pacio and Wetzel (2013) |
| storage implementation | | - | |
| HTF also working fluid | | + | |
| comments | | High heat of evaporation | |

## A.13. Supercritical $H_2O$

Table 15: Detailed HTF Properties - Ultra-Supercritical Direct Steam Generation

| Property | Unit | | |
|---|---|---|---|
| $T_{min}$ (freeze protection) | ℃ | 0 | |
| lower operating $T$ (reference for below) | ℃ | 300 | |
| practical $T_{max}$ (reference for below) | ℃ | 620 | Singer et al. (2010) |
| corresponding pressures | bar | 240 | Singer et al. (2010) |
| density range $\rho$ | kg/m$^3$ | 741–65.1 | Lemmon et al. (2011) |
| isobaric specific thermal capacity $c_p$ | kJ/kg K | (5600–)5.21–2.86 | Lemmon et al. (2011) |
| th. Conductivity $\lambda$ | W/m K | 0.57884–0.10466 | Lemmon et al. (2011) |
| dyn. Viscosity $\mu$ | mPa s | 0.0914–0.0351 | Lemmon et al. (2011) |
| cost | USD/kg | | Pacio and Wetzel (2013) |
| storage implementation | | - | |
| HTF also working fluid | | + | |
| comments | | extrema around critical point | |

## A.14. Supercritical $CO_2$

Table 16: Detailed HTF Properties - supercritical $CO_2$ (s-$CO_2$)

| Property | Unit | | |
|---|---|---|---|
| $T_{min}$ (freeze protection) | ℃ | n.a. | |
| lower operating $T$ (reference for below) | ℃ | 32 | Moisseytsev and Sienicki (2010) |
| practical $T_{max}$ (reference for below) | ℃ | n.a. (850 for reference) | Moisseytsev and Sienicki (2010) |
| corresponding pressures | bar | 78–200 | Moisseytsev and Sienicki (2010) |
| density range $\rho$ | kg/m$^3$ | 881–36.1 | Lemmon et al. (2011) |
| isobaric specific thermal capacity $c_p$ | kJ/kg K | (54.3–)1.28–2.17 | Lemmon et al. (2011) |
| th. Conductivity $\lambda$ | W/m K | 0.0779–0.103 | Lemmon et al. (2011) |
| dyn. Viscosity $\mu$ | mPa s | (0.087–)0.0450–0.0477 | Lemmon et al. (2011) |
| cost | USD/kg | | |
| storage implementation | | - | |
| HTF also working fluid | | + | |
| comments | | low compression work around critical point; high density; extrema around critical point | |

Correlations:

$c_{p,CO_2} = \left[(0.5058+1.359\cdot10^{-3}(T/\mathrm{K})+7.955\cdot10^{-7}(T/\mathrm{K})^2-1.697\cdot10^{-10}(T/\mathrm{K})^3\right]\mathrm{kJ/kg\,K}$ (Cengel and Boles, 2010)

# B. Storage Media

NB: Most of the references are secondary sources.

## B.1. Potential Sensible Heat Storage Media

| Material/Composition (mass-%) | $T_{low}$[°C] | $T_{high}$[°C] | $\rho$ [kg/m$^3$] | $c_p$ [kJ/kg K] | $\lambda$ [W/m K] | price [USD/kg] | Ref. |
|---|---|---|---|---|---|---|---|
| **Liquids** | | | | | | | |
| *Solar Salt*™ | 290 | 593 | 1790 | 1.49–1.54 | 0.50–0.55 | 0.64 | a b |
| $NaNO_3$ | 306 | 700(?) | 1900 | | 0.514 | | c |
| LiF-NaF-KF | 454 | ≈ 1610 | 2200–1800 | 1.89[d] | 0.006–0.01 | 64.06 | e f |
| Saltstream™ 700 | 253 | 700 | 2270–2040 | 1.45[g] | 8.4 [h]; 4.2[i] | [j] | k |
| Na | 97.7 | 873 | 884–745 | 1.27–1.31 | 0.16–0.35 | 2.00 | l m |
| NaK78 | -12.6 | 785 | 779–659 | 0.872–0.893 | 24.1–26.3 | 2.00 | n m |
| Pb-Bi (44.5-55.5) | 125 | 1670 | 10300–8770 | 0.146–0.114 | 12.5–26.6 | 42.23 | f o |
| *Haloglass*$^{TM}$ *RX* | 450 | 1200 | 2400 | 1.36 | 0.8 | | p |



[a] Coastal Chemical Co. (n.d.*b*), Gemasolar (2011), Kopp (2009)
[b] Herrmann and Kearney (2002)
[c] (Yogev and Kribus, 2012; Bauer et al., 2009)
[d] @ 700 °C
[e] Forsberg et al. (2007)
[f] Williams (2006)
[g] @ 300 °C
[h] @ 400 °C
[i] @ 500 °C
[j] "too high for direct storage"
[k] Raade et al. (2012) Halotechnics (2012)
[l] Boerema et al. (2012)
[m] Pacio and Wetzel (2013)
[n] Foust (1972)
[o] Morita et al. (2006)
[p] Halotechnics (2013)

| Material/Composition (mass-%) | $T_{low}$[°C] | $T_{high}$[°C] | $\rho$ [kg/m$^3$] | $c_p$ [kJ/kg K] | $\lambda$ [W/m K] | price [USD/kg] | Ref. |
|---|---|---|---|---|---|---|---|
| **Solids** | | | | | | | |
| 'N4' High-Temperature Concrete | | 500 | 2250[a] | 1.10 [b] | 1.3 | | b c |
| High-Temperature Concrete | | 2680 | 900 | 2.0 | | 0.78–3.18 /kW h$_t$ | d |
| Solid NaCl | | 500 | 2160 | 850 | 7.0 | 0.15 | e |
| Silica Fire Bricks | | 700 | 1820 | 1.00 | 1.5 | 1.0 | e |
| Magnesia Fire Bricks | | 1200 | 3000 | 1.15 | 5.0 | 2.00 | e |
| Ceramics | | $\geq$ 700 | 2400 | 0.85 | 1.3 | | f |
| Graphite | | | 1700 | 1.900 | 200 | | g |
| **Rocks** | | | | | | | |
| Quartzite | | | 2618 | 0.623 | 5.39–3.37[h] | | i |
| Calcareous sandstone | | | 2661 | 0.652 | 4.36–2.98[i] | | i |
| Helvetic siliceous limestone | | | 2776 | 0.669 | 3.60–2.72[i] | | i |
| Limestone | | | 2697 | 0.683 | 2.82–2.05[i] | | i |
| Gabbro | | | 2911 | 0.643 | 2.05 | | i |
| Quartzite Rock | | | 2201 | 0.964 | | | j |

[a] @ 370 °C
[b] Laing, Bahl, Bauer, Fiss, Breidenbach and Hempel (2012)
[c] Laing et al. (2008)
[d] Selvam and Strasser (2012)
[e] Pilkington Solar International GmbH (2000)
[f] Dreißigacker et al. (2013)
[g] Forsberg et al. (2007)
[h] @ 25–175 °C
[i] Zanganeh et al. (2012)
[j] Flueckiger et al. (2011*a*)

| Material/Composition (mass-%) | $T_{low}$[℃] | $T_{high}$[℃] | $\rho$ [kg/m$^3$] | $c_p$ [kJ/kg K] | $\lambda$ [W/m K] | price [USD/kg] | Ref. |
|---|---|---|---|---|---|---|---|
| Steatite (magnesium silicate rock) | | | 2680 | 1.068 | 2.5 | | [k] |
| Granite | | | 2893 | 0.845[l] | 3 | | [m] |
| Dolerite | | | 2657 | 0.839[l] | 3 | | [m] |

[k] Hänchen et al. (2011)
[l] @45 ℃
[m] Allen (2010)

### B.1.1. Haloglass™ RX

Table 19: Some properties of *Haloglass*$^{TM}$ *RX* (Halotechnics, 2013).

| Property | | Value |
|---|---|---|
| Melting Point | | 450 °C |
| Maximum Operating Temperature | | 1200 °C |
| Density | | 2400 kg/m$^3$ |
| $c_p$ at | 450 °C | 1.362 kJ/kg K |
| $\lambda$ | | 0.8 W/m K |
| $\mu$ at | 450 °C | 10 064 mPa s |
| | 600 °C | 600 mPa s |
| | 800 °C | 84.3 mPa s |
| | 1000 °C | 23.6 mPa s |
| | 1200 °C | 11.1 mPa s |

## B.2. PCMs with $T_{\mathrm{melt}} > 550\,^{\circ}\mathrm{C}$

| Composition (mass-%) | $T_{melt}$[°C] | $\Delta h_f$ [kJ/kg] | $\rho$ [kg/m$^3$] | | $c_p$ [kJ/kg K] | | $\lambda$ [W/m K] | | price [USD/kg] | Ref. |
|---|---|---|---|---|---|---|---|---|---|---|
| | | | solid | liquid | solid | liquid | solid | liquid | | |
| **Salts** | | | | | | | | | | |
| $BaCl_2$-CaCl-KCl(47-29-24) | 551 | 219 | 2930 | | 0.67 | 0.84 | | 0.95 | | c |
| $CaCl_2$-$BaCl_2$-KCl(47-29-24)[a] | 551 | 219 | 2930 | | 0.67 | 0.84 | | 0.95 | 0.20 | b |
| CaCl-$CaSO_4$-$CaMoO_4$(38.5-11-4[?])[a] | 673 | 224 | | | | | | | | b |
| $CaF_2$-$CaSO_4$-$CaMoO_4$(49-41.4-9.6)[a] | 943 | 237 | | | | | | | | b |
| $Ca(NO_3)_2$ | 560 | 145 | | | | | | | | c |
| KBr-KF(60-40)[a] | 576 | 315 | | | | | | | | b |
| KBr-$K_2MoO_4$(65-35)[a] | 625 | 90.5 | | | | | | | | b |
| $K_2CO_3$ | 897 | 236 | 2290 | | 2.0 | | | | | h |
| $K_2CO_3$-$Li_2CO_3$-$Na_2CO_3$(62-22-16) | 580 | 288 | 2340 | | 1.80 | 2.09 | | 1.95 | 0.66 | b |
| $K_2CO_3$-$Na_2CO_3$(50-50) | 710 | 163 | | | | | | | | b |
| KCl | 771 | 353 | | | | | | | | c |
| KCl-NaCl-NaF(50.2-39.4-10.4) | 602 | 370.3/m$^3$[i] | | | | | | | | i |
| KF | 857 | 452 | 2370(?) | | | | | | | e |
| KF-$CaF_2$(85-15)[a] | 780 | 440 | | | | | | | | b |
| KF-KCl(55-45)[a] | 605 | 407 | | | | | | | | b |
| KF-$MgF_2$(85-15)[a] | 790 | 520 | | | | | | | | b |
| KF-NaF-$MgF_2$(63.8-27.9-8.3) | 685 | | | 2090 | | | | | | e |

[a] mol.-%
[c] Liu et al. (2012)
[b] Kenisarin (2010)

| Composition (mass-%) | $T_{melt}$[℃] | $\Delta h_f$ [kJ/kg] | $\rho$ [kg/m$^3$] | | $c_p$ [kJ/kg K] | | $\lambda$ [W/m K] | | price [USD/kg] | Ref. |
|---|---|---|---|---|---|---|---|---|---|---|
| | | | solid | liquid | solid | liquid | solid | liquid | | |
| LiCl-$MgF_2$(94.5-5.5)[a] | 573 | 131 | | | | | | | | b |
| LiF | 850 | | | | | | | | | b |
| $Li_2CO_3$-LiF(75.2-24.8) | 595 | 594.5 | | | | | | | | i |
| LiF-$CaF_2$(80.5-19.5)[a] | 767 | 790–820 | 2100 | 2670 | 1.97 | 1.77–1.84 | 1.70–3.8 | 1.70–5.9 | | b c d g |
| LiF-$CeF_3$(80-20)[a] | 756 | 500 | | | | | | | | b |
| LiF-KF-$MgF_2$(74-13-13)[a] | 749 | 860 | | | | | | | | b |
| LiF-$MgF_2$(70-30)[a] | 728 | 520 | | | | | | | | b |
| LiF-$MgF_2$(67-33) | 746 | 947 | 2630(?) | | 1.42 | | 4.66 | | | b |
| LiF-$MgF_2$-KF(64-30-6)[a] | 710 | 782 | | | | | | | | c |
| LiF-NaF(60-40)[a] | 652 | 816 | | | | | | | | b |
| LiF-NaF-$CaF_2$(52-35-13)[a] | 615 | 640 | | | | | | | | b |
| LiF-NaF-$MgF_2$(62-19-19)[a] | 693 | 690 | | | | | | | | b |
| LiF-NaF-$MgF_2$(46-44-10)[a] | 632 | 858 | | | | | | | | b |
| $Li_2SO_4$-$CaSO_4$-$CaMoO_4$(82-11.44-6.56)[a] | 680 | 207 | | | | | | | | b |
| $MgCl_2$ | 714 | 452 | 2140 | | | | | | | e |
| $MgF_2$-KF(70.5-29.5) | 1006 | 770/m$^3$[i] | | | | | | | | i |
| $MgF_2$-LiF(54.2-45.8) | 746 | 847/m$^3$[i] | 2880 | 2305 | | | | | | e |
| $MgF_2$-LiF-$CaF_2$-NaF(37.25–.37.6-34.51–34.79-24.5–25.0-3.21–3.31)[a] | 651–657 | 460–470 | | | | | | | | b |

[i] Gasanaliev and Gamataeva (2000)
[d] Agyenim et al. (2010)

| Composition (mass-%) | $T_{melt}$[°C] | $\Delta h_f$ [kJ/kg] | $\rho$ [kg/m$^3$] | | $c_p$ [kJ/kg K] | | $\lambda$ [W/m K] | | price [USD/kg] | Ref. |
|---|---|---|---|---|---|---|---|---|---|---|
| | | | solid | liquid | solid | liquid | solid | liquid | | |
| $MgF_2$-NaF(69-31) | 996 | 710/m$^3$[i] | | | | | | | | i |
| NaBr-NaF(73-27)[a] | 642 | 360 | | | | | | | | b |
| NaCl | 800 | 467–492 | 2160 | | 5.0 | | | | | c e g |
| NaCl-LiF(76-24) | 680 | 476.9/m$^3$[i] | | | | | | | | i |
| NaCl-NaF(66.5-33.5)[a] | 675 | 572 | | | | | | | | b |
| NaCl-$Na_2MoO_4$-NaBr(38.5-38.5-23)[a] | 612 | 168 | | | | | | | | b |
| NaCl-$NiCl_2$(52-48)[a] | 573 | 558 | | | | | | | | b |
| NaF | 1000 | | | | | | | | 0.74 | b |
| NaF-$CaF_2$(68-32)[a] | 810 | 600 | | | | | | | | b |
| NaF-$CaF_2$-LiF-$MgF_2$(36.5-27.2-25.7-10.6) | 593 | 510/m$^3$ | | | | | | | | i |
| NaF-$CaF_2$-$MgF_2$(65-23-12)[a] | 745 | 568–574 | 1580(?) | | 1.17 | | | | | b |
| NaF-$CaF_2$-$MgF_2$(51.8-34.0-14.2) | 645 | | 2970 | 2370 | | | | | | e |
| NaF-LiF(51.9-48.1) | 652 | 711/m$^3$[i] | 2720 | 1930 | | | | | | e |
| NaF-LiF-$CaF_2$(38.3-35.2-26.5)[a] | 615 | 636 | 2820[j] | | | | | | | b e |
| NaF-LiF-$MgF_2$(50.4-32.6-17)[a] | 622–632 | 625/m$^3$[i] | 2810 | 2105 | | | | | | i e |
| $NaF_2$-LiF-$MgF_2$(49.9-33.4-17.1) | 650 | 860 | 2820(?) | | 1.42 | | 1.15 | | | b |
| NaF-$MgF_2$(75-25) | 832 | 627–650 | 2680(?) | | 1.42 | | 4.66 | | | b |
| NaF-$MgF_2$(66.9-33.1) | 832 | | 2940 | 2190 | | | | | | e |

[j] @ 20 °C

[e] Zalba et al. (2003)

| Composition (mass-%) | $T_{melt}$[°C] | $\Delta h_f$ [kJ/kg] | $\rho$ [kg/m$^3$] | | $c_p$ [kJ/kg K] | | $\lambda$ [W/m K] | | price [USD/kg] | Ref. |
|---|---|---|---|---|---|---|---|---|---|---|
| | | | solid | liquid | solid | liquid | solid | liquid | | |
| NaF-$MgF_2$-KF(64-20-16)[a] | 804 | 650 | | | | | | | | b |
| NaF-$MgF_2$-KF(62.5-22.5-15)[a] | 809 | 543 | | | | | | | | b |
| NaF-$MgF_2$-KF(53.6-28.6-17.8) | 809 | | 2850 | 2110 | | | | | | e |
| $Na_2CO_3$ | 854 | 276 | 2533 | | 2.0 | | | | 2.6 | h |
| $NaCO_3$-$BaCO_3$/MgO | 500–850 | 420 | 2600 | | | | 5.0 | | 2.0 | h |
| $Na_2SO_4$ | 884 | 165 | | | | | | | | c |
| **Metals and metal alloys** | | | | | | | | | | b |
| Al | 660 | 397 | | | | | | | | c |
| Al-Si(12.24-87.76) | 576 | 460–560 | 2540–2700(?) | | 1.038 | 1.741 | 160(?) | 190 | 2.2 | b c f |
| Al-Si(20.0-80.0) | 585 | 460 | | | | | | | | g |
| Al-Si(≥12.6-≤87.4) | 577–1414 | | 2400–2700 | | | | | 60–190(?) | 2.2 | f g |
| Al-Si-Cu(46.3-4.6-49.1) | 571 | 406 | 5560 | | | | | | | c |
| Al-Si-Cu(65-5-30) | 571 | 422 | 2730 | | 1.30 | 1.20 | | | | c |
| Al-Si-Sb(86.4-9.6-4.2) | 575 | 471 | 2700 | | | | | | | c |
| Al-Si-Mg(83.14-11.7-5.16) | 555 | 485 | 2500 | | | | | | | c |
| Cu | 1083 | 193.4 | | | | | | | | c |
| Cu-Si(80-20) | 803 | 197 | 6600 | | 0.50 | | | | | b c |
| Cu-Si-Mg(56-27-17) | 770 | 420 | 4150 | | 0.75 | | | | | b c |
| Cu-P-Si(83-10-7) | 840 | 92 | 6880 | | | | | | | c b |
| Cu-P(91-9) | 715 | 134 | 5600 | | | | | | | c b |

[h] Pilkington Solar International GmbH (2000)
[f] Hunt and Carrington (2012)
[g] Gil et al. (2010)

| Composition (mass-%) | $T_{\mathrm{melt}}$[°C] | $\Delta h_{\mathrm{f}}$ [kJ/kg] | $\rho$ [kg/m$^3$] | | $c_{\mathrm{p}}$ [kJ/kg K] | | $\lambda$ [W/m K] | | price [USD/kg] | Ref. |
|---|---|---|---|---|---|---|---|---|---|---|
| | | | solid | liquid | solid | liquid | solid | liquid | | |
| Cu-Zn-P(69-17-14) | 720 | 368 | 7000 | | | | | | | b c |
| Cu-Zn-Si(74-19-7) | 765 | 125 | 7170 | | | | | | | b c |
| Mg-Ca(84-16) | 790 | 272 | | 1380 | | | | | | b c |
| $Mg_2Cu$ | 841 | 243 | | | | | | | | b |
| Mg-Si-Zn(47-38-15) | 800 | 314 | | | | | | | | b c |
| Si-Mg(56-44) | 946 | 757 | 1900 | | 0.79 | | | | | b c |
| Si-Mg-Ca(49-30-21) | 865 | 305 | 2250 | | | | | | | b c |
| Zn-Cu-Mg(49-45-6) | 703 | 176 | 8670 | | 0.42 | | | | | c |
| $Zn_2Mg$ | 588 | 230 | | | | | | | | b |